Fast multipole method for 3-D Laplace equation in layered media ☆

Bo Wang [a,b], Wenzhong Zhang [b], Wei Cai [b,*]

[a] LCSM(MOE), School of Mathematics and Statistics, Hunan Normal University, Changsha, Hunan, 410081, PR China
[b] Department of Mathematics, Southern Methodist University, Dallas, TX 75275, USA

ARTICLE INFO

ABSTRACT

In this paper, a fast multipole method (FMM) is proposed for 3-D Laplace equations in layered media. The potential due to charges embedded in layered media is decomposed into a free space component and four types of reaction field components, and the latter can be associated with the potential of a polarization source defined for each type. New multipole expansions (MEs) and local expansions (LEs), as well as the multipole to local (M2L) translation operators are derived for the reaction components, based on which FMMs for reaction components are then developed. The resulting FMMs for charge interactions in layered media is a combination of the classic FMM for the free space component and the new FMMs for the reaction field components. With the help of a recurrence formula and contour deformation technique for the run-time computation of the Sommerfeld-type integrals required in M2L translation operators, pre-computations of a large number of tables are avoided. The new FMMs for the reaction components are found to be much faster than the classic FMM for the free space component due to the separation of equivalent polarization charges and target charges by a material interface. As a result, the FMM for potential in layered media costs almost the same as the classic FMM in the free space case. Numerical results validate the fast convergence of the MEs for the reaction components, and the $O(N)$ complexity of the FMMs with a given truncation number p for charge interactions in 3-D layered media.

1. Introduction

Solving Laplace equations in layered media is connected to many important applications in science and engineering. For instance, finding the electric charge distribution over conductors embedded in a layered dielectric medium has important application in semi-conductor industry for calculating the capacitance of interconnects (ICs) in very large-scale integrated (VLSI) circuits for microchip designs (cf. [1–4]). Due to complex geometries of the ICs, the Laplace equation for charge potential is usually solved by an integral method with the Green's function of the layered media (cf. [4,5]), which results in a huge dense linear algebraic system to be solved by an iterative method such as GMRES (cf. [6]), etc. Other applications of the Laplace equation can be found in medical imaging of brains (cf. [7]), elasticity of composite materials (cf. [8]), and electrical impedance tomography for geophysical applications (cf. [9]).

Due to the full matrix resulting from the discretization of integral equations, it will incur an $O(N^2)$ computational cost for computing the product of the matrix with a vector (a basic operation for the GMRES iterative solver). The fast multipole method (FMM) for the free space Green's function (the Coulomb potential) has been used in the development of FastCap (cf. [10]) to accelerate this product to $O(N)$. However, the original FMM of Greengard and Rokhlin (cf. [11,12]) is only designed for the free space Green's function, which reduces the $O(N^2)$ computational cost of N charge interactions in the free space to $O(N)$. To treat the dielectric material interfaces in the IC design, unknowns representing the polarization charges from the dielectric inhomogeneities have to be introduced over the infinite material interfaces, thus creating unnecessary unknowns and contributing to larger linear systems. These extra unknowns over material interfaces can be avoided by using the Green's function of the layered media in the formulation of the integral equations. To find fast algorithms to solve the discretized linear system, image charges are used to approximate the Green's function of the layered media [13–15], converting the reaction potential to the free space Coulomb potential from the charges and their images, thus, the free space FMM can be used [16–18]. Apparently, this approach is limited to the ability of finding image charge approximation for the layered media Green's function. Unfortunately, finding such an image approximation can be challenging, if not impossible, for many layer media.

In this paper, we will develop a FMM for charge interactions in layered media, which can be then used in fast iterative solvers

---

☆ The review of this paper was arranged by Prof. Hazel Andrew.
* Corresponding author.
E-mail address: cai@smu.edu (W. Cai).

for Laplace equations through integral equation methods with a layered media Green's function. We will first derive the multipole expansions (MEs) and local expansions (LEs) for the reaction components for the corresponding layered media Green's function. Then, the original FMM for the interactions of charges in free space will be extended to those of charges embedded in layered media. The approach closely follows our recent work for the Helmholtz equation in layered media (cf. [19,20]), where the generating function of the Bessel function (2-D case) or a Funk–Hecke formula (3-D case) were used to connect Bessel functions and plane wave functions in order to derive the MEs, LEs, and M2L operators. The reason of using Fourier (2-D case) and spherical harmonic (3-D case) expansions of plane waves is that the Green's function of layered media has a Sommerfeld-type integral representation also involving the plane waves. Even though the Laplace equation could be considered as a zero limit of the wave number k in the Helmholtz equation, special treatments of the $k \to 0$ limit are required to obtain a limit version of the extended Funk–Hecke formula, which is the key in the derivation of MEs, LEs, and M2L for the reaction components of the Laplacian Green's function in layered media. Similar to our previous work for the Helmholtz equation in layered media, the potential due to sources embedded in layered media is decomposed into free space and reaction components and equivalent polarization charges are introduced to re-express the reaction components. The FMM in layered media will then consist of classic FMM for the free space components and FMMs for reaction components, using equivalent polarization sources and the new MEs, LEs, and M2L translations. Moreover, for fast and accurate calculations of the Sommerfeld integrals in the M2L translation operators, especially for charges very close to material interfaces, and to avoid making pre-computed tables (cf. [19]), we will introduce a recurrence formula as well as special integration contour deformation techniques. As in the Helmholtz equation case, the FMMs for the reaction field components are much faster than that for the free space components due to the fact that the introduced equivalent polarization charges are always separated from target charges by a material interface. As a result, the new FMM for charges in layered media costs almost the same as the classic FMM for the free space case.

The rest of the paper is organized as follows. In Section 2, we will consider the limit case of the extended Funk–Hecke formula introduced in [19], which leads to a spherical harmonic expansion of the exponential kernel in the Sommerfeld-type integral representation of the Green's function. By using this expansion, we present new alternative derivations, via the Fourier spectral domain, for the ME, LE, and M2L operators of the free space Green's function. The same approach will be then used to derive MEs, LEs, and M2L translation operators for the reaction components of the layered Green's function. In Section 3, after a short discussion on the Green's function in layered media consisting of free space and reaction components, we present the formulas for the potential induced by sources embedded in layered media. Then, the concept of equivalent polarization charge of a source charge is introduced for each type of the reaction components. The reaction components of the layered Green's function and the potential are then re-expressed by using the equivalent polarization charges. Further, we derive the MEs, LEs, and M2L translation operators for the reaction components based on expressions using equivalent polarization charges. Combining the original source charges and the equivalent polarization charges associated to each reaction component, the FMMs for reaction components can be implemented. A recurrence formula and contour deformation techniques are also introduced for the computation of M2L operator related Sommerfeld integrals. Section 4 will give numerical results to show the spectral accuracy

and $O(N)$ complexity of the proposed FMM for charge interactions in layered media. A conclusion is given in Section 5 while two appendices are included for addition theorems and a recursive algorithm for computing reaction field density in the spectral domain.

2. A new derivation for the multipole and local expansions for the far field potential of charges in free space

In this section, we first briefly review the main idea of the free space FMM and the conventional derivations of the key formulas, i.e., the multipole and local expansions of the free space Green's function of the Laplace equation, and the corresponding shifting and translation operators. Then, we present a new derivation for all the formulas by using the Sommerfeld-type integral representation of the Green's function. The key expansion used in the new derivation is a limiting case of the extended Funk–Hecke formula introduced in [19]. This new technique shall be applied to derive MEs and LEs for the reaction components of the layered media Green's function later on.

2.1. An introduction of the fast multipole method (FMM) in free space

Given N source charges $\{Q_j\}_{j=1}^N$ at locations $\{\boldsymbol{r}_j'\}_{j=1}^N$, consider the calculation of the Coulombic potential

$$\Phi(\boldsymbol{r}) = \sum_{j=1}^N \frac{Q_j}{|\boldsymbol{r} - \boldsymbol{r}_j'|}, \tag{2.1}$$

at N target points $\{\boldsymbol{r} = \boldsymbol{r}_i\}_{i=1}^N$. Obviously, this can be seen as the interactions of N charges if the target points $\{\boldsymbol{r}_i\}_{i=1}^N$ are exactly the source locations $\{\boldsymbol{r}_j'\}_{j=1}^N$ (in this case, the sum will not include the singular self-interaction term). Direct computation leads to an $O(N^2)$ cost while the FMM is a fast method which reduces the cost to $O(N)$.

The key technique in the FMM is the multipole expansion (ME) for the far field of the potential. Suppose the source charges $\{Q_j, \boldsymbol{r}_j'\}_{j=1}^N$ are enclosed in a sphere of radius a centered at $\boldsymbol{r}_c^s$, the far field potential in the FMM framework refers to the potential at target points with a distance to the center of the sphere greater than $2a$. In such a scenery, the combined potential from all source charges could be represented by one source, at the center of the sphere, with multipole source components beyond the mono-pole of the Coulombic potential, such as dipole, quadrupole, etc.

To illustrate how this can be achieved, we need to introduce the multipole expansion at the center $\boldsymbol{r}_c^s$ of a sphere for the Coulombic potential of one single source charge at any given point $\boldsymbol{r}'$ inside the sphere, see Fig. 2.1. Given any point $\boldsymbol{r}$ far away from the source point $\boldsymbol{r}'$, the law of cosines gives

$$|\boldsymbol{r} - \boldsymbol{r}'|^2 = r^2 + (r')^2 - 2rr' \cos\gamma, \tag{2.2}$$

where (r, θ, φ) and (r', θ', φ') are the spherical coordinates of $\boldsymbol{r}, \boldsymbol{r}'$ and the angle between them is γ,

$$\cos\gamma = \cos\theta \cos\theta' + \sin\theta \sin\theta' \cos(\varphi - \varphi'). \tag{2.3}$$

Then, the Coulomb potential of a unit charge at $\boldsymbol{r}'$ in the free space is represented by the Green's function of the Laplace equation

$$G(\boldsymbol{r}, \boldsymbol{r}') = \frac{1}{|\boldsymbol{r} - \boldsymbol{r}'|} = \frac{1}{r\sqrt{1 - 2\mu\cos\gamma + \mu^2}}$$

$$= \frac{1}{r'\sqrt{1 - 2\frac{\cos\gamma}{\mu} + \frac{1}{\mu^2}}}, \tag{2.4}$$

where $\mu = r'/r$ and the scaling constant $1/4\pi$ has been omitted through out this paper. Furthermore, we have the following Taylor expansions

$$\frac{1}{r\sqrt{1 - 2\mu\cos\gamma + \mu^2}} = \sum_{n=0}^{\infty} P_n(\cos\gamma)\frac{\mu^n}{r} = \sum_{n=0}^{\infty} P_n(\cos\gamma)\frac{r'^n}{r^{n+1}},$$
$$\text{for} \quad \mu < 1,$$
(2.5)

and

$$\frac{1}{r'\sqrt{1 - 2\frac{\cos\gamma}{\mu} + \frac{1}{\mu^2}}} = \sum_{n=0}^{\infty} P_n(\cos\gamma)\frac{1}{r'\mu^n} = \sum_{n=0}^{\infty} P_n(\cos\gamma)\frac{r^n}{r'^{n+1}},$$
$$\text{for} \quad \mu > 1.$$
(2.6)

By using the fact $|P_n(x)| \leq 1$, $x \in [-1, 1]$, the expansions above have exponential convergence

$$\left| \frac{1}{|\boldsymbol{r} - \boldsymbol{r}'|} - \sum_{n=0}^{p} \frac{P_n(\cos\gamma)(r')^n}{r^{n+1}} \right| \leq \frac{1}{r - r'}\left(\frac{r'}{r}\right)^{p+1}, \quad r > r', \quad (2.7)$$

and

$$\left| \frac{1}{|\boldsymbol{r} - \boldsymbol{r}'|} - \sum_{n=0}^{p} P_n(\cos\gamma)\frac{r^n}{(r')^{n+1}} \right| \leq \frac{1}{r' - r}\left(\frac{r}{r'}\right)^{p+1}, \quad r < r'.$$
(2.8)

Let $\boldsymbol{r}_c^t$ be a target center close to $\boldsymbol{r}$ and $\boldsymbol{r}_c^s$ be a source center close to $\boldsymbol{r}'$ and assume $|\boldsymbol{r}' - \boldsymbol{r}_c^s| < |\boldsymbol{r} - \boldsymbol{r}_c^s|$ and $|\boldsymbol{r}' - \boldsymbol{r}_c^t| > |\boldsymbol{r} - \boldsymbol{r}_c^t|$, see Fig. 2.1. Following the derivation in (2.2)–(2.6), we have Taylor expansions

$$\frac{1}{|\boldsymbol{r} - \boldsymbol{r}'|} = \frac{1}{|(\boldsymbol{r} - \boldsymbol{r}_c^s) - (\boldsymbol{r}' - \boldsymbol{r}_c^s)|} = \sum_{n=0}^{\infty} \frac{P_n(\cos\gamma_s)}{r_s}\left(\frac{r'_s}{r_s}\right)^n, \quad (2.9)$$

and

$$\frac{1}{|\boldsymbol{r} - \boldsymbol{r}'|} = \frac{1}{|(\boldsymbol{r} - \boldsymbol{r}_c^t) - (\boldsymbol{r}' - \boldsymbol{r}_c^t)|} = \sum_{n=0}^{\infty} \frac{P_n(\cos\gamma_t)}{r'_t}\left(\frac{r_t}{r'_t}\right)^n, \quad (2.10)$$

where $(r_s, \theta_s, \varphi_s)$, $(r_t, \theta_t, \varphi_t)$ are the spherical coordinates of $\boldsymbol{r} - \boldsymbol{r}_c^s$ and $\boldsymbol{r} - \boldsymbol{r}_c^t$, $(r'_s, \theta'_s, \varphi'_s)$, $(r'_t, \theta'_t, \varphi'_t)$ are the spherical coordinates of $\boldsymbol{r}' - \boldsymbol{r}_c^s$ and $\boldsymbol{r}' - \boldsymbol{r}_c^t$ (see Fig. 2.1) and

$$\cos\gamma_s = \cos\theta_s\cos\theta'_s + \sin\theta_s\sin\theta'_s\cos(\varphi_s - \varphi'_s),$$
$$\cos\gamma_t = \cos\theta_t\cos\theta'_t + \sin\theta_t\sin\varphi'_t\cos(\varphi_t - \varphi'_t).$$
(2.11)

Note that $P_n(\cos\gamma_s)$, $P_n(\cos\gamma_t)$ still mix the source and target information ($\boldsymbol{r}$ and $\boldsymbol{r}'$). Applying Legendre addition Theorem A.1 to expansions (2.9) and (2.10) gives a ME

$$\frac{1}{|\boldsymbol{r} - \boldsymbol{r}'|} = \sum_{n=0}^{\infty}\sum_{m=-n}^{n} M_{nm} r_s^{-n-1} Y_n^m(\theta_s, \varphi_s), \quad (2.12)$$

and a LE

$$\frac{1}{|\boldsymbol{r} - \boldsymbol{r}'|} = \sum_{n=0}^{\infty}\sum_{m=-n}^{n} L_{nm} r_t^n Y_n^m(\theta_t, \varphi_t), \quad (2.13)$$

where

$$M_{nm} = c_n^{-2} r_s'^n \overline{Y_n^m(\theta'_s, \varphi'_s)}, \quad L_{nm} = c_n^{-2} r_t'^{-n-1} \overline{Y_n^m(\theta'_t, \varphi'_t)}, \quad (2.14)$$

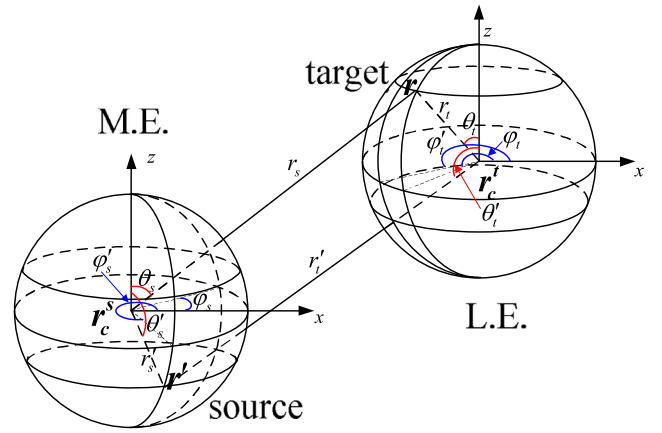and, Y_n^m and c_n are defined in (A.1) and (A.5), respectively.

Fig. 2.1. Spherical coordinates used in multipole and local expansions.

Applying the ME (2.12) to each term in the potential (2.1) gives approximation

$$\Phi(\boldsymbol{r}) \approx \sum_{n=0}^{p}\sum_{m=-n}^{n} \widetilde{M}_{nm} r_s^{-n-1} Y_n^m(\theta_s, \varphi_s), \quad (2.15)$$

where the coefficients, which only depend on the location and magnitude of the sources, are defined as

$$\widetilde{M}_{nm} = c_n^{-2}\sum_{j=1}^{N} Q_j r_{sj}'^n \overline{Y_n^m(\theta'_{sj}, \varphi'_{sj})}, \quad (2.16)$$

where $(r'_{sj}, \theta'_{sj}, \varphi'_{sj})$ are the spherical coordinates of $\boldsymbol{r}'_j - \boldsymbol{r}_c^s$ and p is the truncation order of the ME. By error estimate (2.7), the approximation (2.15) has exponential convergence as

$$\left| \Phi(\boldsymbol{r}) - \sum_{n=0}^{p}\sum_{m=-n}^{n} \widetilde{M}_{nm} r_s^{-n-1} Y_n^m(\theta_s, \varphi_s) \right| \leq \frac{1}{2^{p+1}a}\sum_{j=1}^{N} Q_j,$$
$$\forall \boldsymbol{r} \text{ s.t. } |\boldsymbol{r} - \boldsymbol{r}_c^s| \geq 2a. \quad (2.17)$$

Therefore, we can have a low rank approximation for the far field of the potential $\Phi(\boldsymbol{r})$, i.e., (2.15) with small integer p. This implies a fast linear cost method to compute potential at N far field target locations $\{\boldsymbol{r}_i\}_{i=1}$. The fast method is implemented in the following two steps:

Step 1: Pre-compute the ME coefficients $\widetilde{M}_{nm}$ in (2.16) with a cost of $O(p^2 N)$, $0 \leq n \leq p$, $-n \leq m \leq n$.
Step 2: Applying (2.15) to compute $\{\Phi(\boldsymbol{r}_i)\}_{i=1}^N$ at a cost of $O(p^2 N)$.

We can see that the overall cost for computing $\{\Phi(\boldsymbol{r}_i)\}_{i=1}^N$ by using the ME approximation will be $O(N)$ instead of $O(N^2)$ using a direct evaluation of the potential function in (2.1).

Note that the fast method described above requires the target locations to be well separated from the source sphere. However, such a condition will not hold in many N-body interaction problems as the source and target charges are usually the same set of charges. Realizing the convergence result (2.17) of the ME approximation holds for any scale a, the FMM utilizes an octree hierarchical structure to partition a box containing all the source and target charges and applies the low rank compression (2.15) between any two boxes of a given scale a as long as they are separated by distance a, namely, non-adjacent boxes.

In the FMM implementation, there will be one upward and one downward recursive loops traversing the tree structure. An **upward loop** along the tree is used to compute the MEs of all boxes starting from the smallest boxes of the tree (the lowest

level of the tree, the root of the tree taken as the highest level). Once the MEs for the boxes at the lowest level are computed according to (2.16), the ME of each box in the up next level can be simply obtained by merging the MEs of its eight children with the help of a M2M (ME to ME) shifting operator, which relates the ME coefficients of two MEs at two different centers. Next, a **downward loop** along the tree will be used to compute the local expansion (LE) of all boxes, which represents the potential due to charges outside a given box and its eight neighboring boxes. This time, the loop starts from the largest box (namely, the largest box containing all charges) whose local expansion (LE) is zero as there is no charges outside. In the downward loop for the LEs, a shifting for the LE at the center of a box to those at the centers of its children will be needed. This can be done by a L2L (local to local) shifting operator, which relates the LE coefficients of two LEs at two different centers. In the downward loop for the LEs, we will also need to translate MEs of boxes in the interaction list of a given box to LEs at the centers of this box. This leads to the ME to LE (M2L) translation operator, which translate the ME coefficients of the far field of a group of charges to the LE coefficients of a LE at the center of a far field target box.

The final step of the FMM is to compute the potential in each one of the boxes at the lowest level of the tree (i.e., the smallest boxes), which combines the LE of the box, the outcome of the downward loop, and the potential contributions from charges in the eight children of the box via direct calculations. For the algorithmic details, please refer to [11,21,22].

All the shifting and translation operators mentioned above can be derived by using the addition theorems in Appendix A, which are summarized as follows.

- **M2L translation.** Applying the addition Theorem A.3 to expansion functions in ME (2.12) provides a translation from ME (2.12) to LE (2.13) as follows

$$L_{nm} = \sum_{n'=0}^{\infty} \sum_{m'=-n'}^{n'} \frac{(-1)^{n'+m} A_{n'}^{m'} A_n^m Y_{n+n'}^{m'-m}(\theta_{st}, \varphi_{st})}{c_{n'}^2 A_{n+n'}^{m'-m} r_{st}^{n+n'+1}} M_{n'm'}, \quad (2.18)$$

where $(r_{st}, \theta_{st}, \varphi_{st})$ is the spherical coordinate of $\boldsymbol{r}_c^s - \boldsymbol{r}_c^t$.

- **M2M and L2L translations.**

$$\tilde{M}_{nm} = \sum_{n'=0}^{n} \sum_{m'=-n'}^{n'} \frac{(-1)^{m'} A_{n'}^{m'} A_{n-n'}^{m-m'} r_{ss}^{n'} Y_{n'}^{-m'}(\theta_{ss}, \varphi_{ss})}{c_{n'}^2 A_n^m} M_{n-n',m-m'}, \quad (2.19)$$

$$\tilde{L}_{nm} = \sum_{n'=n}^{\infty} \sum_{m'=-n'}^{n'} \frac{(-1)^{n'-n} c_{n'}^2 A_{n'-n}^{m'-m} A_n^m r_{tt}^{n'-n} Y_{n'-n}^{m'-m}(\theta_{tt}, \varphi_{tt})}{c_{n'-n}^2 c_n^2 A_{n'}^{m'}} L_{n'm'}, \quad (2.20)$$

can be derived by using addition Theorems A.2 and A.4. Here, $(r_{ss}, \theta_{ss}, \varphi_{ss})$ and $(r_{tt}, \theta_{tt}, \varphi_{tt})$ are the spherical coordinates of $\boldsymbol{r}_c^s - \tilde{\boldsymbol{r}}_c^s$ and $\boldsymbol{r}_c^t - \tilde{\boldsymbol{r}}_c^t$,

$$\tilde{M}_{nm} = c_n^{-2} \tilde{r}_s'^n \overline{Y_n^m(\tilde{\theta}_s', \tilde{\varphi}_s')}, \quad \tilde{L}_{nm} = c_n^{-2} \tilde{r}_t'^{-n-1} \overline{Y_n^m(\tilde{\theta}_t', \tilde{\varphi}_t')}, \quad (2.21)$$

are the ME and LE coefficients with respect to new centers $\tilde{\boldsymbol{r}}_c^s$ and $\tilde{\boldsymbol{r}}_c^t$, respectively.

2.2. A new derivation of the multipole and local expansions in the free space

Besides using the addition theorems as in the previous section, the target/source separation in (2.12) can also be achieved in the Fourier spectral domain. We shall give an alternative new derivation for (2.12) and (2.13) by using the integral representation of

$1/|\boldsymbol{r} - \boldsymbol{r}'|$. The main motivation for this effort is that it can be further applied to derive multipole and local expansions for the reaction components of the Green's function in layered media to be discussed in Section 3.

For the Green's function $G(\boldsymbol{r}, \boldsymbol{r}')$, we have the well known identity

$$\frac{1}{|\boldsymbol{r} - \boldsymbol{r}'|} = \frac{1}{2\pi} \int_0^\infty \int_0^{2\pi} e^{ik_\rho((x-x')\cos\alpha + (y-y')\sin\alpha) - k_\rho|z-z'|} d\alpha dk_\rho. \quad (2.22)$$

By this identity, we straightforwardly have source/target separation in spectral domain as follows

$$\frac{1}{|\boldsymbol{r} - \boldsymbol{r}'|} = \frac{1}{2\pi} \int_0^\infty \int_0^{2\pi} e^{ik_\rho \boldsymbol{k}_0 \cdot (\boldsymbol{r} - \boldsymbol{r}_c^s)} e^{-ik_\rho \boldsymbol{k}_0 \cdot (\boldsymbol{r}' - \boldsymbol{r}_c^s)} d\alpha dk_\rho,$$

$$\frac{1}{|\boldsymbol{r} - \boldsymbol{r}'|} = \frac{1}{2\pi} \int_0^\infty \int_0^{2\pi} e^{ik_\rho \boldsymbol{k}_0 \cdot (\boldsymbol{r} - \boldsymbol{r}_c^t)} e^{-ik_\rho \boldsymbol{k}_0 \cdot (\boldsymbol{r}' - \boldsymbol{r}_c^t)} d\alpha dk_\rho, \quad (2.23)$$

for $z \geq z'$ where

$$\boldsymbol{k}_0 = (\cos\alpha, \sin\alpha, i), \quad (2.24)$$

and without loss of generality, here we only consider the case $z \geq z'$ as an example.

A FMM for the Helmholtz kernel in layered media has been proposed in [19] based on a similar source/target separation in the spectral domain. One of the key ingredients is the following extension of the well-known Funk–Hecke formula (cf. [23,24]).

Proposition 2.1. *Given* $\boldsymbol{r} = (x, y, z) \in \mathbb{R}^3$, $k > 0$, $\alpha \in [0, 2\pi)$ *and denoted by* (r, θ, φ) *the spherical coordinates of* $\boldsymbol{r}$, $\boldsymbol{k} = (\sqrt{k^2 - k_z^2} \cos\alpha, \sqrt{k^2 - k_z^2} \sin\alpha, k_z)$ *is a vector of complex entries. Choosing branch* (2.26) *for* $\sqrt{k^2 - k_z^2}$ *in* $e^{i\boldsymbol{k}\cdot\boldsymbol{r}}$ *and* $\widehat{P}_n^m(\frac{k_z}{k})$ *as defined in* (A.1), *then*

$$e^{i\boldsymbol{k}\cdot\boldsymbol{r}} = \sum_{n=0}^{\infty} \sum_{m=-n}^{n} A_n^m(\boldsymbol{r}) i^n \widehat{P}_n^m\left(\frac{k_z}{k}\right) e^{-im\alpha}$$

$$= \sum_{n=0}^{\infty} \sum_{m=-n}^{n} \overline{A_n^m(\boldsymbol{r})} i^n \widehat{P}_n^m\left(\frac{k_z}{k}\right) e^{im\alpha}, \quad (2.25)$$

holds for all $k_z \in \mathbb{C}$, *where*

$$A_n^m(\boldsymbol{r}) = 4\pi j_n(kr) Y_n^m(\theta, \varphi).$$

This extension enlarges the range of the classic Funk–Hecke formula from $k_z \in (-k, k)$ to the whole complex plane by choosing the branch

$$\sqrt{k^2 - k_z^2} = -i\sqrt{r_1 r_2} e^{i\frac{\theta_1 + \theta_2}{2}}, \quad (2.26)$$

for the square root function $\sqrt{k^2 - k_z^2}$. Here (r_i, θ_i), $i = 1, 2$ are the modules and principal values of the arguments of complex numbers $k_z + k$ and $k_z - k$, i.e.,

$$k_z + k = r_1 e^{i\theta_1}, \quad -\pi < \theta_1 \leq \pi, \quad k_z - k = r_2 e^{i\theta_2}, \quad -\pi < \theta_2 \leq \pi.$$

It is worthy to point out that the normalized associated Legendre function $\widehat{P}_n^m(x)$ has also been extended to the whole complex plane by using the same branch.

Although we have $k_\rho \boldsymbol{k}_0 = \lim_{k\to 0^+}(\sqrt{k^2 - k_z^2}\cos\alpha, \sqrt{k^2 - k_z^2}\sin\alpha, k_z)$, with $k_z = ik_\rho$, taking limit directly in the expansion (2.25) will induce singularity in the associated Legendre function. In the following, we will show how to cancel the singularity to obtain a limit version of (2.25), which gives an expansion for $e^{ik_\rho \boldsymbol{k}_0 \cdot \boldsymbol{r}}$. For this purpose, we first recall the corresponding extended Legendre addition theorem (cf. [19]).

Lemma 2.1. *Let* $\boldsymbol{w} = (\sqrt{1-w^2}\cos\alpha, \sqrt{1-w^2}\sin\alpha, w)$ *be a vector with complex entries,* θ, φ *be the azimuthal angle and polar angles of a unit vector* $\hat{\boldsymbol{r}}$. *Define*

$$\beta(w) = w\cos\theta + \sqrt{1-w^2}\sin\theta\cos(\alpha - \varphi), \qquad (2.27)$$

then

$$P_n(\beta(w)) = \frac{4\pi}{2n+1}\sum_{m=-n}^{n}\widehat{P}_n^m(\cos\theta)\widehat{P}_n^m(w)e^{im(\alpha-\varphi)}, \qquad (2.28)$$

for all $w \in \mathbb{C}$.

From this extended Legendre addition theorem, the following expansion can be obtained by choosing a specific $\boldsymbol{\omega}$ and then taking limit carefully.

Lemma 2.2. *Let* $\boldsymbol{k}_0 = (\cos\alpha, \sin\alpha, i)$ *be a vector with complex entry,* θ, φ *be the azimuthal angle and polar angles of a unit vector* $\hat{\boldsymbol{r}}$. *Then*

$$\frac{(i\boldsymbol{k}_0\cdot\hat{\boldsymbol{r}})^n}{n!} = \sum_{m=-n}^{n}C_n^m\widehat{P}_n^m(\cos\theta)e^{im(\alpha-\varphi)}, \qquad (2.29)$$

where

$$C_n^m = i^{2n-m}\sqrt{\frac{4\pi}{(2n+1)(n+m)!(n-m)!}}. \qquad (2.30)$$

Proof. For any $k \in \mathbb{R}^+$, define $\boldsymbol{k} = (\sqrt{k^2+1}\cos\alpha, \sqrt{k^2+1}\sin\alpha, i)$. By Lemma 2.1, we have

$$k^n P_n\left(\frac{\boldsymbol{k}\cdot\hat{\boldsymbol{r}}}{k}\right) = \frac{4\pi}{2n+1}\sum_{m=-n}^{n}\widehat{P}_n^m(\cos\theta)k^n\widehat{P}_n^m\left(\frac{i}{k}\right)e^{im(\alpha-\varphi)}. \qquad (2.31)$$

Consider the limit of the above identity as $k \to 0^+$. Note that

$$\lim_{k\to 0^+}\boldsymbol{k}\cdot\hat{\boldsymbol{r}} = \boldsymbol{k}_0\cdot\hat{\boldsymbol{r}}, \qquad (2.32)$$

together with the knowledge on the coefficient of the leading term in the Legendre polynomial $P_n(x)$ lead to

$$\lim_{k\to 0^+}k^n P_n\left(\frac{\boldsymbol{k}\cdot\hat{\boldsymbol{r}}}{k}\right) = \frac{(2n)!}{2^n(n!)^2}(\boldsymbol{k}_0\cdot\hat{\boldsymbol{r}})^n. \qquad (2.33)$$

Recall the Rodrigues' formula of the associated Legendre function

$$\widehat{P}_n^m(x) = \frac{c_{nm}}{2^n n!}(1-x^2)^{\frac{m}{2}}\frac{d^{n+m}}{dx^{n+m}}(x^2-1)^n, \quad c_{nm} = \sqrt{\frac{2n+1}{4\pi}\frac{(n-m)!}{(n+m)!}} \qquad (2.34)$$

for $0 \le m \le n$, we have

$$k^n\widehat{P}_n^m\left(\frac{i}{k}\right) = \frac{c_{nm}}{2^n n!}\frac{(2n)!}{(n-m)!}(k^2+1)^{\frac{m}{2}}\cdot k^{n-m}\widetilde{Q}_{n-m}\left(\frac{i}{k}\right) \qquad (2.35)$$

where $\widetilde{Q}_n(z)$ is a *monic* polynomial of degree n. Hence, we get similarly

$$\lim_{k\to 0^+}k^n\widehat{P}_n^m\left(\frac{i}{k}\right) = \frac{c_{nm}}{2^n n!}\frac{(2n)!i^{n-m}}{(n-m)!}. \qquad (2.36)$$

The identity $\widehat{P}_n^{-m}(x) = (-1)^m\widehat{P}_n^m(x)$ will give the limit for $-n \le m < 0$ cases. Now, let $k \to 0^+$ in (2.31) and use results (2.33) and (2.36), we complete the proof. $\square$

Proposition 2.2. *Given* $\boldsymbol{r} = (x, y, z) \in \mathbb{R}^3$, $\alpha \in [0, 2\pi)$ *and denoted by* (r, θ, φ) *the spherical coordinates of* $\boldsymbol{r}$, $\boldsymbol{k}_0 =$

$(\cos\alpha, \sin\alpha, i)$ *is a vector of complex entries. Then*

$$e^{ik_\rho\boldsymbol{k}_0\cdot\boldsymbol{r}} = \sum_{n=0}^{\infty}\sum_{m=-n}^{n}C_n^m r^n Y_n^m(\theta, \varphi)k_\rho^n e^{-im\alpha}$$

$$= \sum_{n=0}^{\infty}\sum_{m=-n}^{n}C_n^m r^n \overline{Y_n^m(\theta, \varphi)}k_\rho^n e^{im\alpha}, \qquad (2.37)$$

holds for all $r > 0$, $k_\rho > 0$, *where* C_n^m *is the constant defined in* (2.30).

Proof. By Taylor expansion, we have

$$e^{ik_\rho\boldsymbol{k}_0\cdot\boldsymbol{r}} = \sum_{n=0}^{\infty}\frac{(i\boldsymbol{k}_0\cdot\hat{\boldsymbol{r}})^n}{n!}k_\rho^n r^n. \qquad (2.38)$$

Then, (2.37) follows by applying Lemma 2.2 to each term in the above expansion. $\square$

Remark 2.1. By setting $k_z = ik_\rho$ and using the limit values given by (2.33) and (2.36), one can also verify that the expansions for $e^{ik_\rho\boldsymbol{k}_0\cdot\boldsymbol{r}}$ in Proposition 2.2 are exactly the limiting cases of the expansions in Proposition 2.1.

Applying spherical harmonic expansion (2.37) to exponential functions $e^{-ik_\rho\boldsymbol{k}_0\cdot(\boldsymbol{r}-\boldsymbol{r}_c^s)}$ and $e^{ik\cdot(\boldsymbol{r}-\boldsymbol{r}_c^t)}$ in (2.23) gives

$$\frac{1}{|\boldsymbol{r}-\boldsymbol{r}'|} = \sum_{n=0}^{\infty}\sum_{m=-n}^{n}M_{nm}\frac{(-1)^n c_n^2 C_n^m}{2\pi}$$

$$\times \int_0^\infty\int_0^{2\pi}k_\rho^n e^{ik_\rho\boldsymbol{k}_0\cdot(\boldsymbol{r}-\boldsymbol{r}_c^s)}e^{im\alpha}d\alpha dk_\rho, \qquad (2.39)$$

and

$$\frac{1}{|\boldsymbol{r}-\boldsymbol{r}'|} = \sum_{n=0}^{\infty}\sum_{m=-n}^{n}\hat{L}_{nm}r_t^n Y_n^m(\theta_t, \varphi_t), \qquad (2.40)$$

for $z \ge z'$, where M_{nm} is defined in (2.14) and

$$\hat{L}_{nm} = \frac{C_n^m}{2\pi}\int_0^\infty\int_0^{2\pi}k_\rho^n e^{ik_\rho\boldsymbol{k}_0\cdot(\boldsymbol{r}_c^t-\boldsymbol{r}')}e^{-im\alpha}d\alpha dk_\rho. \qquad (2.41)$$

Recall the identity

$$r^{-n-1}Y_n^{-m}(\theta, \varphi) = \frac{(-1)^n c_n^2 C_n^m}{2\pi}\int_0^\infty\int_0^{2\pi}k_\rho^n e^{ik_\rho\boldsymbol{k}_0\cdot\boldsymbol{r}}e^{-im\alpha}d\alpha dk_\rho, \qquad (2.42)$$

for $z \ge 0$, we see that (2.39) and (2.40) are exactly the ME (2.12) and LE (2.13) in the case of $z \ge z'$.

To derive the translation from the ME (2.12) to the LE (2.13), we perform further splitting

$$e^{ik_\rho\boldsymbol{k}_0\cdot(\boldsymbol{r}-\boldsymbol{r}_c^s)} = e^{ik_\rho\boldsymbol{k}_0\cdot(\boldsymbol{r}-\boldsymbol{r}_c^t)}e^{ik_\rho\boldsymbol{k}_0\cdot(\boldsymbol{r}_c^t-\boldsymbol{r}_c^s)}, \qquad (2.43)$$

in (2.39) and apply expansion (2.37) again to obtain the translation

$$L_{nm} = C_n^m\sum_{n'=0}^{\infty}\sum_{m'=-n'}^{n'}M_{n'm'}\frac{(-1)^{n'}c_{n'}^2 C_{n'}^{m'}}{2\pi}$$

$$\times \int_0^\infty\int_0^{2\pi}k_\rho^{n+n'}e^{ik_\rho\boldsymbol{k}_0\cdot(\boldsymbol{r}_c^t-\boldsymbol{r}_c^s)}e^{i(m'-m)\alpha}d\alpha dk_\rho.$$

By using the identity (2.42), we can also verify that the above integral form is equal to the entries of the M2L translation matrix defined in (2.18).
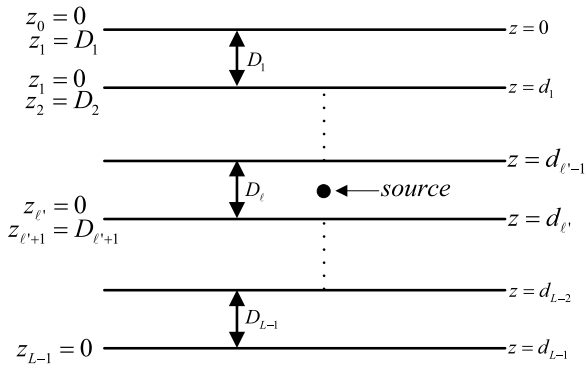
Fig. 3.1. Sketch of the layer structure for general multi-layer media.

3. FMM for 3-D Laplace equation in layered media

In this section, the potential of charges in layered media is formulated using layered Green's function and then decomposed into a free space component and four types of reaction components. Furthermore, the reaction components are re-expressed by using equivalent polarization charges. The new expressions are used to derive the MEs and LEs for the reaction components of the layered Green's function in the same spirit as in the last section. Based on these new expansions and translations, FMM for 3-D Laplace kernel in layered media can be developed.

3.1. Potential due to sources embedded in multi-layer media

Consider a layered medium consisting of L-interfaces located at $z = d_\ell, \ell = 0, 1, \ldots, L-1$, see Fig. 3.1. The piecewise constant material parameter is described by $\{\varepsilon_\ell\}_{\ell=0}^L$. Suppose we have a point source at $\mathbf{r}' = (x', y', z')$ in the ℓ'th layer ($d_{\ell'} < z' < d_{\ell'-1}$), then, the layered media Green's function $u_{\ell\ell'}(\mathbf{r}, \mathbf{r}')$ for the Laplace equation satisfies

$$\Delta u_{\ell\ell'}(\mathbf{r}, \mathbf{r}') = -\delta(\mathbf{r}, \mathbf{r}'), \tag{3.1}$$

at field point $\mathbf{r} = (x, y, z)$ in the ℓth layer ($d_\ell < z < d_{\ell-1}$) where $\delta(\mathbf{r}, \mathbf{r}')$ is the Dirac delta function. By using Fourier transforms along x- and y-directions, the problem can be solved analytically for each layer in z by imposing transmission conditions at the interface between ℓth and $(\ell - 1)$th layer ($z = d_{\ell-1}$), i.e.,

$$u_{\ell-1,\ell'}(x, y, z) = u_{\ell\ell'}(x, y, z),$$
$$\varepsilon_{\ell-1} \frac{\partial u_{\ell-1,\ell'}(x, y, z)}{\partial z} = \varepsilon_\ell \frac{\partial u_{\ell\ell'}(k_x, k_y, z)}{\partial z}, \tag{3.2}$$

as well as the decaying conditions in the top and bottom-most layers as $z \to \pm\infty$.

Here, we give the expression for the analytic solution with detailed derivations included in Appendix B. In general, the layered media Green's function in the physical domain takes the form

$$u_{\ell\ell'}(\mathbf{r}, \mathbf{r}') = \begin{cases} u_{\ell\ell'}^r(\mathbf{r}, \mathbf{r}') + \dfrac{1}{4\pi|\mathbf{r} - \mathbf{r}'|}, & \ell = \ell', \\ u_{\ell\ell'}^r(\mathbf{r}, \mathbf{r}'), & \text{otherwise}, \end{cases} \tag{3.3}$$

where

$$u_{\ell\ell'}^r(\mathbf{r}, \mathbf{r}') = \begin{cases} u_{0\ell'}^{11}(\mathbf{r}, \mathbf{r}') + u_{0\ell'}^{12}(\mathbf{r}, \mathbf{r}'), \\ u_{\ell\ell'}^{11}(\mathbf{r}, \mathbf{r}') + u_{\ell\ell'}^{12}(\mathbf{r}, \mathbf{r}') + u_{\ell\ell'}^{21}(\mathbf{r}, \mathbf{r}') + u_{\ell\ell'}^{22}(\mathbf{r}, \mathbf{r}'), \\ \quad 0 < \ell < L, \\ u_{L\ell'}^{21}(\mathbf{r}, \mathbf{r}') + u_{L\ell'}^{22}(\mathbf{r}, \mathbf{r}'). \end{cases}$$
$$\tag{3.4}$$

The reaction component $u_{\ell\ell'}^{\mathfrak{ab}}(\mathbf{r}, \mathbf{r}')$ is given in an integral form

$$u_{\ell\ell'}^{\mathfrak{ab}}(\mathbf{r}, \mathbf{r}') = \frac{1}{8\pi^2} \int_0^\infty \int_0^{2\pi} e^{i\mathbf{k}_\alpha \cdot (\boldsymbol{\rho} - \boldsymbol{\rho}')} \mathcal{Z}_{\ell\ell'}^{\mathfrak{ab}}(z, z')$$
$$\times \sigma_{\ell\ell'}^{\mathfrak{ab}}(k_\rho) d\alpha dk_\rho, \quad \mathfrak{a}, \mathfrak{b} = 1, 2, \tag{3.5}$$

where,

$$\mathbf{k}_\alpha = k_\rho(\cos\alpha, \sin\alpha), \tag{3.6}$$

and $\{\mathcal{Z}_{\ell\ell'}^{\mathfrak{ab}}(z, z')\}_{\mathfrak{a}, \mathfrak{b}=1}^2$ are exponential functions defined as

$$\mathcal{Z}_{\ell\ell'}^{11}(z, z') := e^{-k_\rho(z - d_\ell + z' - d_{\ell'})}, \quad \mathcal{Z}_{\ell\ell'}^{12}(z, z') := e^{-k_\rho(z - d_\ell + d_{\ell'-1} - z')},$$
$$\mathcal{Z}_{\ell\ell'}^{21}(z, z') := e^{-k_\rho(d_{\ell-1} - z + z' - d_{\ell'})}, \quad \mathcal{Z}_{\ell\ell'}^{22}(z, z') := e^{-k_\rho(d_{\ell-1} - z + d_{\ell'-1} - z')},$$
$$\tag{3.7}$$

$\{\sigma_{\ell\ell'}^{\mathfrak{ab}}(k_\rho)\}_{\mathfrak{a}, \mathfrak{b}=1}^2$ are reaction densities only dependent on the layer structure and the material parameter k_ℓ in each layer. The reaction densities can be calculated efficiently by using a recursive algorithm, see Appendix B for more details. It is worthwhile to point out that the reaction components $u_{\ell\ell'}^{\mathfrak{a}2}$ or $u_{\ell\ell'}^{\mathfrak{a}1}$ will vanish if the source $\mathbf{r}'$ is in the top or bottom most layer.

With the expression of the Green's function in layered media, we are ready to consider the potential due to sources in layered media. Let $\mathscr{P}_\ell = \{(Q_{\ell j}, \mathbf{r}_{\ell j}), j = 1, 2, \ldots, N_\ell\}, \ell = 0, 1, \ldots, L$ be L groups of source charges distributed in a multi-layer medium with $L + 1$ layers (see Fig. 3.1). The group of charges in ℓth layer is denoted by $\mathscr{P}_\ell$. Apparently, the potential at $\mathbf{r}_{\ell i}$ due to all other charges is given by the summation

$$\Phi_\ell(\mathbf{r}_{\ell i}) = \sum_{\ell'=0}^L \sum_{j=1}^{N_{\ell'}} Q_{\ell' j} u_{\ell\ell'}(\mathbf{r}_{\ell i}, \mathbf{r}_{\ell' j}) = \sum_{j=1, j\neq i}^{N_\ell} \frac{Q_{\ell j}}{4\pi|\mathbf{r}_{\ell i} - \mathbf{r}_{\ell j}|}$$
$$+ \sum_{\ell'=0}^L \sum_{j=1}^{N_{\ell'}} Q_{\ell' j} u_{\ell\ell'}^r(\mathbf{r}_{\ell i}, \mathbf{r}_{\ell' j}), \tag{3.8}$$

where $u_{\ell\ell'}^r(\mathbf{r}, \mathbf{r}')$ are the reaction field components defined in (3.4)–(3.7). As the reaction components of the Green's function in multi-layer media have different expressions (3.5) for sources and targets in different layers, it is necessary to perform calculation individually for interactions between any two groups of charges among the $L + 1$ groups $\{\mathscr{P}_\ell\}_{\ell=0}^L$. Applying expressions (3.4) and (3.5) in (3.8), we obtain

$$\Phi_\ell(\mathbf{r}_{\ell i}) = \Phi_\ell^{\text{free}}(\mathbf{r}_{\ell i}) + \Phi_\ell^r(\mathbf{r}_{\ell i})$$
$$= \Phi_\ell^{\text{free}}(\mathbf{r}_{\ell i}) + \sum_{\ell'=0}^{L-1} [\Phi_{\ell\ell'}^{11}(\mathbf{r}_{\ell i}) + \Phi_{\ell\ell'}^{21}(\mathbf{r}_{\ell i})]$$
$$+ \sum_{\ell'=1}^L [\Phi_{\ell\ell'}^{12}(\mathbf{r}_{\ell i}) + \Phi_{\ell\ell'}^{22}(\mathbf{r}_{\ell i})], \tag{3.9}$$

where

$$\Phi_\ell^{\text{free}}(\mathbf{r}_{\ell i}) := \sum_{j=1, j\neq i}^{N_\ell} \frac{Q_{\ell j}}{4\pi|\mathbf{r}_{\ell i} - \mathbf{r}_{\ell j}|}, \quad \Phi_{\ell\ell'}^{\mathfrak{ab}}(\mathbf{r}_{\ell i}) := \sum_{j=1}^{N_{\ell'}} Q_{\ell' j} u_{\ell\ell'}^{\mathfrak{ab}}(\mathbf{r}_{\ell i}, \mathbf{r}_{\ell' j}).$$
$$\tag{3.10}$$

According to (3.9), the potential due to charges in layered media has L free space and $4(L^2 - 2L + 1)$ reaction components. Obviously, all free space components $\Phi_\ell^{\text{free}}(\mathbf{r}_{\ell i})$ can be computed using the traditional FMM. Thus, the main task of this paper is to develop FMMs for the reaction components $\{\Phi_{\ell\ell'}^{\mathfrak{ab}}(\mathbf{r}_{\ell i})\}_{\mathfrak{a}, \mathfrak{b}=1}^2$. The key step to achieve this task is to derive MEs, LEs and corresponding shifting and translation operators for the reaction components defined in (3.5).

3.2. Equivalent polarization sources for reaction components

The expressions of the components given in (3.10) show that the free space components only involve interactions between charges in the same layer. Interactions between charges in different layers are all included in the reaction components. Two groups of charges involved in the computation of a reaction component could be physically very far away from each other as there could be many layers between the source and target layers associated to the reaction component, see Fig. 3.2 (left).

Our recent work on the Helmholtz equation [19,20], of which the Laplace equation can be considered as a special case where the wave number $k = 0$, has shown that the exponential convergence of the ME and LE for the reaction components $u_{\ell\ell'}^{\mathfrak{ab}}(\mathbf{r}, \mathbf{r}')$ in fact depends on the distance between the target charge $\mathbf{r}$ and a polarization charge defined for the source charge $\mathbf{r}'$, which uses the distance between the source charge $\mathbf{r}'$ and the nearest material interface and always locates next to the nearest interface adjacent to the target charge. Fig. 3.3 illustrates the location of the polarization charge $\mathbf{r}'_{\mathfrak{ab}}$ for each of the four types of reaction fields $\tilde{u}_{\ell\ell'}^{\mathfrak{ab}}$, $\mathfrak{a}, \mathfrak{b} = 1, 2$. Specifically, the equivalent polarization sources associated to reaction components $u_{\ell\ell'}^{\mathfrak{ab}}(\mathbf{r}, \mathbf{r}')$, $\mathfrak{a}, \mathfrak{b} = 1, 2$ are set to be at coordinates (see Fig. 3.3)

$$\mathbf{r}'_{11} := (x', y', d_\ell - (z' - d_{\ell'})), \qquad \mathbf{r}'_{12} := (x', y', d_\ell - (d_{\ell'-1} - z')),$$
$$\mathbf{r}'_{21} := (x', y', d_{\ell-1} + (z' - d_{\ell'})), \quad \mathbf{r}'_{22} := (x', y', d_{\ell-1} + (d_{\ell'-1} - z')),$$
$$(3.11)$$

and the reaction potentials are

$$\tilde{u}_{\ell\ell'}^{\mathfrak{ab}}(\mathbf{r}, \mathbf{r}'_{\mathfrak{ab}}) := \frac{1}{8\pi^2} \int_0^\infty \int_0^{2\pi} e^{i\mathbf{k}_\alpha \cdot (\boldsymbol{\rho} - \boldsymbol{\rho}')} e^{-k_\rho |z - z'_{\mathfrak{ab}}|}$$
$$\times \sigma_{\ell\ell'}^{\mathfrak{ab}}(k_\rho) d\alpha dk_\rho, \quad \mathfrak{a}, \mathfrak{b} = 1, 2, \quad (3.12)$$

where $z'_{\mathfrak{ab}}$ denotes the z-coordinate of $\mathbf{r}'_{\mathfrak{ab}}$, i.e.,

$$z'_{11} = d_\ell - (z' - d_{\ell'}), \ z'_{12} = d_\ell - (d_{\ell'-1} - z'),$$
$$z'_{21} = d_{\ell-1} + (z' - d_{\ell'}), \ z'_{22} = d_{\ell-1} + (d_{\ell'-1} - z').$$

We can see that the reaction potentials (3.12) represented by the equivalent polarization sources has similar form as the Sommerfeld-type integral representation (2.22) of the free space Green's function except for the extra density functions $\sigma_{\ell\ell'}^{\mathfrak{ab}}(k_\rho)$. Moreover, recall the definition in (3.11) we have

$$z > z'_{1\mathfrak{b}}, \quad \text{and} \quad z < z'_{2\mathfrak{b}}, \quad \mathfrak{b} = 1, 2.$$

Therefore, the absolute value in the integral form (3.12) can be removed according to the index $\mathfrak{a}$. More precisely, define

$$\mathcal{E}^+(\mathbf{r}, \mathbf{r}') := e^{i\mathbf{k}_\alpha \cdot (\boldsymbol{\rho} - \boldsymbol{\rho}')} e^{k_\rho(z - z')}, \quad \mathcal{E}^-(\mathbf{r}, \mathbf{r}') := e^{i\mathbf{k}_\alpha \cdot (\boldsymbol{\rho} - \boldsymbol{\rho}')} e^{-k_\rho(z - z')}, \quad (3.13)$$

then

$$\tilde{u}_{\ell\ell'}^{1\mathfrak{b}}(\mathbf{r}, \mathbf{r}'_{1\mathfrak{b}}) = \frac{1}{8\pi^2} \int_0^\infty \int_0^{2\pi} \mathcal{E}^-(\mathbf{r}, \mathbf{r}'_{1\mathfrak{b}}) \sigma_{\ell\ell'}^{1\mathfrak{b}}(k_\rho) d\alpha dk_\rho,$$
$$\tilde{u}_{\ell\ell'}^{2\mathfrak{b}}(\mathbf{r}, \mathbf{r}'_{2\mathfrak{b}}) = \frac{1}{8\pi^2} \int_0^\infty \int_0^{2\pi} \mathcal{E}^+(\mathbf{r}, \mathbf{r}'_{2\mathfrak{b}}) \sigma_{\ell\ell'}^{2\mathfrak{b}}(k_\rho) d\alpha dk_\rho.$$

Recall the expressions (3.7), we verify that

$$\mathcal{E}^-(\mathbf{r}, \mathbf{r}'_{1\mathfrak{b}}) = e^{i\mathbf{k}_\alpha \cdot (\boldsymbol{\rho} - \boldsymbol{\rho}')} \mathcal{Z}_{\ell\ell'}^{1\mathfrak{b}}(z, z'),$$
$$\mathcal{E}^+(\mathbf{r}, \mathbf{r}'_{2\mathfrak{b}}) = e^{i\mathbf{k}_\alpha \cdot (\boldsymbol{\rho} - \boldsymbol{\rho}')} \mathcal{Z}_{\ell\ell'}^{2\mathfrak{b}}(z, z'), \quad \mathfrak{b} = 1, 2. \quad (3.14)$$

Therefore, the reaction components (3.5) is equal to the reaction potentials defined for associated equivalent polarization sources, i.e.,

$$u_{\ell\ell'}^{1\mathfrak{b}}(\mathbf{r}, \mathbf{r}') = \tilde{u}_{\ell\ell'}^{1\mathfrak{b}}(\mathbf{r}, \mathbf{r}'_{1\mathfrak{b}}), \quad u_{\ell\ell'}^{2\mathfrak{b}}(\mathbf{r}, \mathbf{r}') = \tilde{u}_{\ell\ell'}^{2\mathfrak{b}}(\mathbf{r}, \mathbf{r}'_{2\mathfrak{b}}), \quad \mathfrak{b} = 1, 2.$$

$$(3.15)$$

A substitution into the expression of $\Phi_{\ell\ell'}^{\mathfrak{ab}}(\mathbf{r}_{\ell i})$ in (3.10) leads to

$$\Phi_{\ell\ell'}^{\mathfrak{ab}}(\mathbf{r}_{\ell i}) = \sum_{j=1}^{N_{\ell'}} Q_{\ell'j} \tilde{u}_{\ell\ell'}^{\mathfrak{ab}}(\mathbf{r}_{\ell i}, \mathbf{r}_{\ell'j}^{\mathfrak{ab}}), \quad \mathfrak{a}, \mathfrak{b} = 1, 2, \quad (3.16)$$

where

$$\mathbf{r}_{\ell'j}^{11} = (x_{\ell'j}, y_{\ell'j}, d_\ell - (z_{\ell j} - d_{\ell'})),$$
$$\mathbf{r}_{\ell'j}^{12} = (x_{\ell'j}, y_{\ell'j}, d_\ell - (d_{\ell'-1} - z_{\ell j})),$$
$$\mathbf{r}_{\ell'j}^{21} = (x_{\ell'j}, y_{\ell'j}, d_{\ell-1} + (z_{\ell j} - d_{\ell'})),$$
$$\mathbf{r}_{\ell'j}^{22} = (x_{\ell'j}, y_{\ell'j}, d_{\ell-1} + (d_{\ell'-1} - z_{\ell j})),$$
$$(3.17)$$

are coordinates of the associated equivalent polarization sources for the computation of reaction components $\Phi_{\ell\ell'}^{\mathfrak{ab}}(\mathbf{r}_{\ell i})$, see Fig. 3.2 for an illustration of $\{\mathbf{r}_{\ell'j}^{11}\}_{j=1}^{N_{\ell'}}$ and $\{\mathbf{r}_{\ell'j}^{21}\}_{j=1}^{N_{\ell'}}$.

By using the expression (3.16), the computation of the reaction components can be performed between targets and associated equivalent polarization sources. The definition given by (3.17) shows that the target particles $\{\mathbf{r}_{\ell i}\}_{i=1}^{N_\ell}$ and the corresponding equivalent polarization sources are always located on different sides of an interface $z = d_{\ell-1}$ or $z = d_\ell$, see Fig. 3.2. We still emphasize that the introduced equivalent polarization sources are separate with the target charges even in considering the reaction components for source and target charges in the same layer, see the numerical examples given in Section 3.4. This property implies significant advantage of introducing equivalent polarization sources and using expression (3.16) in the FMMs for the reaction components $\Phi_{\ell\ell'}^{\mathfrak{ab}}(\mathbf{r}_{\ell i})$, $\mathfrak{a}, b = 1, 2$. The numerical results presented in Section 4 show that the FMMs for reaction components have high efficiency as a direct consequence of the separation of the targets and equivalent polarization sources by interface.

3.3. The fast multipole algorithm

In the development of FMM for reaction components $\Phi_{\ell\ell'}^{\mathfrak{ab}}(\mathbf{r}_{\ell i})$, we will adopt the expression (3.16) with equivalent polarization sources. Therefore, multipole and local expansions and corresponding translation operators for $\tilde{u}_{\ell\ell'}^{\mathfrak{ab}}(\mathbf{r}, \mathbf{r}'_{\mathfrak{ab}})$ are derived first. Inspired by source/target separation in (2.23), similar separations

$$\mathcal{E}^-(\mathbf{r}, \mathbf{r}'_{1\mathfrak{b}}) = \mathcal{E}^-(\mathbf{r}, \mathbf{r}_c^{1\mathfrak{b}}) e^{i\mathbf{k}_\alpha \cdot (\boldsymbol{\rho}_c^{1\mathfrak{b}} - \boldsymbol{\rho}') - k_\rho(z_c^{1\mathfrak{b}} - z'_{1\mathfrak{b}})},$$
$$\mathcal{E}^+(\mathbf{r}, \mathbf{r}'_{2\mathfrak{b}}) = \mathcal{E}^+(\mathbf{r}, \mathbf{r}_c^{2\mathfrak{b}}) e^{i\mathbf{k}_\alpha \cdot (\boldsymbol{\rho}_c^{2\mathfrak{b}} - \boldsymbol{\rho}') + k_\rho(z_c^{2\mathfrak{b}} - z'_{2\mathfrak{b}})},$$
$$(3.18)$$

and

$$\mathcal{E}^-(\mathbf{r}, \mathbf{r}'_{1\mathfrak{b}}) = \mathcal{E}^-(\mathbf{r}_c^t, \mathbf{r}'_{1\mathfrak{b}}) e^{i\mathbf{k}_\alpha \cdot (\boldsymbol{\rho} - \boldsymbol{\rho}_c^t) - k_\rho(z - z_c^t)},$$
$$\mathcal{E}^+(\mathbf{r}, \mathbf{r}'_{2\mathfrak{b}}) = \mathcal{E}^+(\mathbf{r}_c^t, \mathbf{r}'_{2\mathfrak{b}}) e^{i\mathbf{k}_\alpha \cdot (\boldsymbol{\rho} - \boldsymbol{\rho}_c^t) + k_\rho(z - z_c^t)},$$
$$(3.19)$$

for $\mathfrak{b} = 1, 2$ are introduced by inserting the source center $\mathbf{r}_c^{\mathfrak{ab}} = (x_c^{\mathfrak{ab}}, y_c^{\mathfrak{ab}}, z_c^{\mathfrak{ab}})$ and the target center $\mathbf{r}_c^t = (x_c^t, y_c^t, z_c^t)$, respectively. Here, we also use notations $\boldsymbol{\rho}_c^{\mathfrak{ab}} = (x_c^{\mathfrak{ab}}, y_c^{\mathfrak{ab}})$, $\boldsymbol{\rho}_c^t = (x_c^t, y_c^t)$ for coordinates projected in xy-plane. Now, applying Proposition 2.2 gives us the following spherical harmonic expansions:

$$e^{i\mathbf{k}_\alpha \cdot (\boldsymbol{\rho}_c^{2\mathfrak{b}} - \boldsymbol{\rho}'_{2\mathfrak{b}}) + k_\rho(z_c^{2\mathfrak{b}} - z'_{2\mathfrak{b}})} = \sum_{n=0}^\infty \sum_{m=-n}^n C_n^m (r_c^{2\mathfrak{b}})^n \overline{Y_n^m(\theta_c^{2\mathfrak{b}}, \pi + \varphi_c^{2\mathfrak{b}})} k_\rho^n e^{im\alpha},$$

$$e^{i\mathbf{k}_\alpha \cdot (\boldsymbol{\rho}_c^{1\mathfrak{b}} - \boldsymbol{\rho}'_{1\mathfrak{b}}) - k_\rho(z_c^{1\mathfrak{b}} - z'_{1\mathfrak{b}})} = \sum_{n=0}^\infty \sum_{m=-n}^n C_n^m (r_c^{1\mathfrak{b}})^n \overline{Y_n^m(\pi - \theta_c^{1\mathfrak{b}}, \pi + \varphi_c^{1\mathfrak{b}})} k_\rho^n e^{im\alpha},$$

$$(3.20)$$

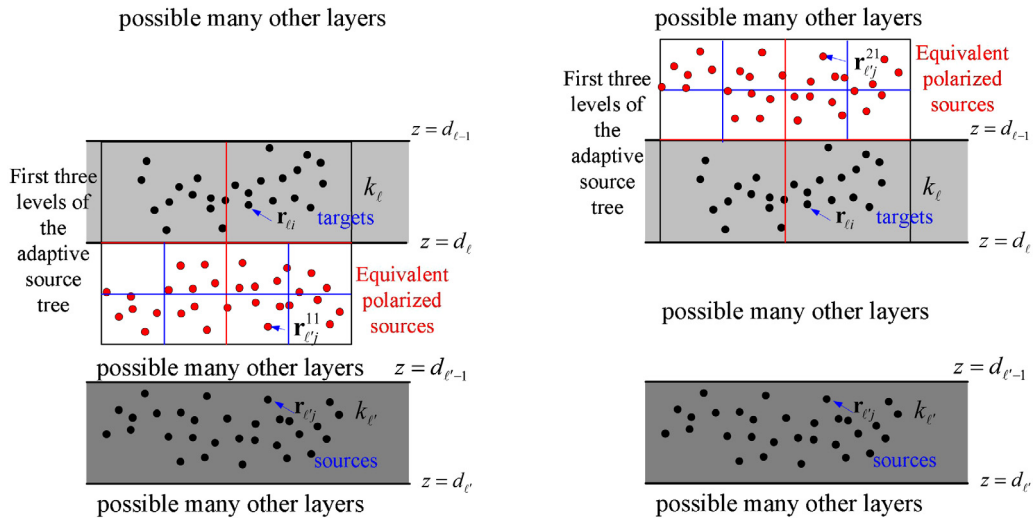**Fig. 3.2.** Equivalent polarized sources $\{r_{\ell'j}^{11}\}$, $\{r_{\ell'j}^{21}\}$ and boxes in source tree.
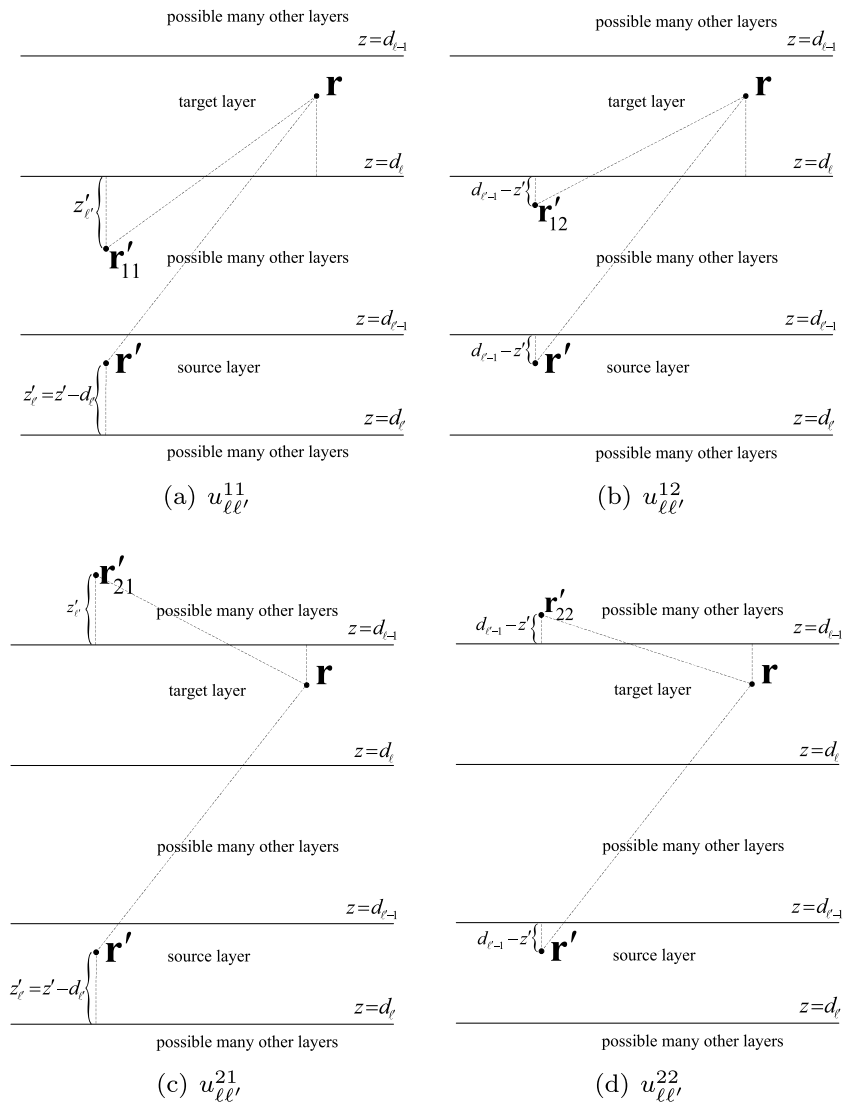

Fig. 3.3. Location of equivalent polarization sources for the computation of $u_{\ell\ell'}^{ab}$.

and

$$e^{i\mathbf{k}_\alpha \cdot (\boldsymbol{\rho}-\boldsymbol{\rho}_c^t)-k_\rho(z-z_c^t)} = \sum_{n=0}^{\infty} \sum_{m=-n}^{n} C_n^m r_t^n Y_n^m(\theta_t, \varphi_t) k_\rho^n e^{-im\alpha},$$

$$e^{i\mathbf{k}_\alpha \cdot (\boldsymbol{\rho}-\boldsymbol{\rho}_c^t)+k_\rho(z-z_c^t)} = \sum_{n=0}^{\infty} \sum_{m=-n}^{n} C_n^m r_t^n Y_n^m(\pi - \theta_t, \varphi_t) k_\rho^n e^{-im\alpha},$$

(3.21)

where $(r_c^{\mathfrak{ab}}, \theta_c^{\mathfrak{ab}}, \varphi_c^{\mathfrak{ab}})$ is the spherical coordinates of $\mathbf{r}'_{\mathfrak{ab}} - \mathbf{r}_c^{\mathfrak{ab}}$. By equalities

$$Y_n^m(\pi - \theta, \varphi) = (-1)^{n+m} Y_n^m(\theta, \varphi),$$
$$Y_n^m(\theta, \pi + \varphi) = (-1)^m Y_n^m(\theta, \varphi),$$

the above spherical harmonic expansions (3.20)–(3.21) together with source/target separation (3.18) and (3.19) lead to

$$\mathcal{E}^-(\mathbf{r}, \mathbf{r}'_{1\mathfrak{b}}) = \mathcal{E}^-(\mathbf{r}, \mathbf{r}_c^{1\mathfrak{b}}) \sum_{n=0}^{\infty} \sum_{m=-n}^{n} (-1)^n C_n^m (r_c^{1\mathfrak{b}})^n \overline{Y_n^m(\theta_c^{1\mathfrak{b}}, \varphi_c^{1\mathfrak{b}})} k_\rho^n e^{im\alpha},$$

$$\mathcal{E}^+(\mathbf{r}, \mathbf{r}'_{2\mathfrak{b}}) = \mathcal{E}^+(\mathbf{r}, \mathbf{r}_c^{2\mathfrak{b}}) \sum_{n=0}^{\infty} \sum_{m=-n}^{n} (-1)^m C_n^m (r_c^{2\mathfrak{b}})^n \overline{Y_n^m(\theta_c^{2\mathfrak{b}}, \varphi_c^{2\mathfrak{b}})} k_\rho^n e^{im\alpha},$$

(3.22)

and

$$\mathcal{E}^-(\mathbf{r}, \mathbf{r}'_{1\mathfrak{b}}) = \mathcal{E}^-(\mathbf{r}_c^t, \mathbf{r}'_{1\mathfrak{b}}) \sum_{n=0}^{\infty} \sum_{m=-n}^{n} C_n^m r_t^n Y_n^m(\theta_t, \varphi_t) k_\rho^n e^{-im\alpha},$$

$$\mathcal{E}^+(\mathbf{r}, \mathbf{r}'_{2\mathfrak{b}}) = \mathcal{E}^+(\mathbf{r}_c^t, \mathbf{r}'_{2\mathfrak{b}}) \sum_{n=0}^{\infty} \sum_{m=-n}^{n} (-1)^{n+m} C_n^m r_t^n Y_n^m(\theta_t, \varphi_t) k_\rho^n e^{-im\alpha},$$

(3.23)

for $\mathfrak{b} = 1, 2$. Then, a substitution of (3.22) and (3.23) into (3.15) gives a ME

$$\tilde{u}_{\ell\ell'}^{\mathfrak{ab}}(\mathbf{r}, \mathbf{r}'_{\mathfrak{ab}}) = \sum_{n=0}^{\infty} \sum_{m=-n}^{n} M_{nm}^{\mathfrak{ab}} \widetilde{\mathcal{F}}_{nm}^{\mathfrak{ab}}(\mathbf{r}, \mathbf{r}_c^{\mathfrak{ab}}),$$

$$M_{nm}^{\mathfrak{ab}} = c_n^{-2} (r_c^{\mathfrak{ab}})^n Y_n^m(\theta_c^{\mathfrak{ab}}, \varphi_c^{\mathfrak{ab}}),$$

(3.24)

at equivalent polarization source centers $\mathbf{r}_c^{\mathfrak{ab}}$ and LE

$$\tilde{u}_{\ell\ell'}^{\mathfrak{ab}}(\mathbf{r}, \mathbf{r}'_{\mathfrak{ab}}) = \sum_{n=0}^{\infty} \sum_{m=-n}^{n} L_{nm}^{\mathfrak{ab}} r_t^n Y_n^m(\theta_t, \varphi_t)$$

(3.25)

at target center $\mathbf{r}_c^t$, respectively. Here, $\widetilde{\mathcal{F}}_{nm}^{\mathfrak{ab}}(\mathbf{r}, \mathbf{r}_c^{\mathfrak{ab}})$ are given in forms of Sommerfeld-type integrals

$$\widetilde{\mathcal{F}}_{nm}^{1\mathfrak{b}}(\mathbf{r}, \mathbf{r}_c^{1\mathfrak{b}}) = \frac{(-1)^n c_n^2 C_n^m}{8\pi^2} \int_0^{\infty} \int_0^{2\pi} \mathcal{E}^-(\mathbf{r}, \mathbf{r}_c^{1\mathfrak{b}}) \sigma_{\ell\ell'}^{1\mathfrak{b}}(k_\rho) k_\rho^n e^{im\alpha} d\alpha dk_\rho,$$

$$\widetilde{\mathcal{F}}_{nm}^{2\mathfrak{b}}(\mathbf{r}, \mathbf{r}_c^{2\mathfrak{b}}) = \frac{(-1)^m c_n^2 C_n^m}{8\pi^2} \int_0^{\infty} \int_0^{2\pi} \mathcal{E}^+(\mathbf{r}, \mathbf{r}_c^{2\mathfrak{b}}) \sigma_{\ell\ell'}^{2\mathfrak{b}}(k_\rho) k_\rho^n e^{im\alpha} d\alpha dk_\rho,$$

(3.26)

and the LE coefficients are given by

$$L_{nm}^{1\mathfrak{b}} = \frac{C_n^m}{8\pi^2} \int_0^{\infty} \int_0^{2\pi} \mathcal{E}^-(\mathbf{r}_c^t, \mathbf{r}'_{1\mathfrak{b}}) \sigma_{\ell\ell'}^{1\mathfrak{b}}(k_\rho) k_\rho^n e^{-im\alpha} d\alpha dk_\rho,$$

$$L_{nm}^{2\mathfrak{b}} = \frac{(-1)^{n+m} C_n^m}{8\pi^2} \int_0^{\infty} \int_0^{2\pi} \mathcal{E}^+(\mathbf{r}_c^t, \mathbf{r}'_{2\mathfrak{b}}) \sigma_{\ell\ell'}^{2\mathfrak{b}}(k_\rho) k_\rho^n e^{-im\alpha} d\alpha dk_\rho.$$

(3.27)

Let us give some numerical examples to show the convergence behavior of finite truncated MEs in (3.24). Consider the MEs of $\tilde{u}_{11}^{11}(\mathbf{r}, \mathbf{r}'_{11})$ and $\tilde{u}_{11}^{22}(\mathbf{r}, \mathbf{r}'_{22})$ in a three-layer media with $\varepsilon_0 = 21.2$,

$\varepsilon_1 = 47.5$, $\varepsilon_2 = 62.8$, $d_0 = 0$, $d_1 = -1.2$. In all the following examples, we fix $\mathbf{r}' = (0.625, 0.5, -0.1)$ in the middle layer and use definition (3.11) to determine $\mathbf{r}'_{11} = (0.625, 0.5, -2.3)$, $\mathbf{r}'_{22} = (0.625, 0.5, 0.1)$. The centers for MEs are set to be $\mathbf{r}_c^{11} = (0.6, 0.6, -2.4)$, $\mathbf{r}_c^{22} = (0.6, 0.6, 0.2)$ which implies $|\mathbf{r}'_{11} - \mathbf{r}_c^{11}| = |\mathbf{r}'_{22} - \mathbf{r}_c^{22}| \approx 0.1436$. For both components, we shall test three targets given as follows

$$\mathbf{r}_1 = (0.5, 0.625, -0.1), \quad \mathbf{r}_2 = (0.5, 0.625, -0.6),$$
$$\mathbf{r}_3 = (0.5, 0.625, -1.1).$$

The relative errors against truncation number p are depicted in Fig. 3.4. We also plot the convergence rates similar with that of the ME of free space Green's function, i.e., $O\left[\left(\frac{|\mathbf{r}-\mathbf{r}_c^{\mathfrak{ab}}|}{|\mathbf{r}'_{\mathfrak{ab}}-\mathbf{r}_c^{\mathfrak{ab}}|}\right)^{p+1}\right]$ as reference convergence rates. The results clearly show that the MEs of the reaction components $u_{11}^{\mathfrak{ab}}(\mathbf{r}, \mathbf{r}'_{\mathfrak{ab}})$ have spectral convergence rate $O\left[\left(\frac{|\mathbf{r}-\mathbf{r}_c^{\mathfrak{ab}}|}{|\mathbf{r}'_{\mathfrak{ab}}-\mathbf{r}_c^{\mathfrak{ab}}|}\right)^{p+1}\right]$ similar as that of free space Green's function. Actually, their exponential convergence has been determined by the Euclidean distance between target and polarization source. Therefore, the MEs (3.24) can be used to develop FMM for efficient computation of the reaction components as in the development of classic FMM for the free space Green's function.

According to the definition of $\mathcal{E}^-(\mathbf{r}, \mathbf{r}')$ and $\mathcal{E}^+(\mathbf{r}, \mathbf{r}')$ in (3.14), the centers $\mathbf{r}_c^t$ and $\mathbf{r}_c^{\mathfrak{ab}}$ have to satisfy

$$z_c^{1\mathfrak{b}} < d_\ell, \quad z_c^{2\mathfrak{b}} > d_{\ell-1}, \quad z_c^t > d_\ell \text{ for } \tilde{u}_{\ell\ell'}^{1\mathfrak{b}}(\mathbf{r}, \mathbf{r}'_{1\mathfrak{b}});$$
$$z_c^t < d_{\ell-1} \text{ for } \tilde{u}_{\ell\ell'}^{2\mathfrak{b}}(\mathbf{r}, \mathbf{r}'_{2\mathfrak{b}}),$$

(3.28)

to ensure the exponential decay in $\mathcal{E}^-(\mathbf{r}, \mathbf{r}_c^{1\mathfrak{b}})$, $\mathcal{E}^+(\mathbf{r}, \mathbf{r}_c^{2\mathfrak{b}})$ and $\mathcal{E}^-(\mathbf{r}_c^t, \mathbf{r}'_{1\mathfrak{b}})$, $\mathcal{E}^+(\mathbf{r}_c^t, \mathbf{r}'_{2\mathfrak{b}})$ as $k_\rho \to \infty$ and hence the convergence of the corresponding Sommerfeld-type integrals in (3.26) and (3.27). These restrictions can be met easily in practice, as we are considering targets in the ℓth layer and the equivalent polarized coordinates are always located either above the interface $z = d_{\ell-1}$ or below the interface $z = d_\ell$. More details will be discussed below in the presentation of the FMM algorithm.

We still need to consider the center shifting and translation operators for ME (3.24) and LE (3.25). A desirable feature of the expansions of reaction components discussed above is that the formula (3.24) for the ME coefficients and the formula (3.25) for the LE have exactly the same form as the formulas of ME coefficients and LE for the free space Green's function. Therefore, the center shifting for MEs and LEs of reaction components are exactly the same as free space case given in (2.19)–(2.20).

Next, we derive the translation operator from the ME (3.24) to the LE (3.25). Recall the definition of exponential functions in (3.13), $\mathcal{E}^-(\mathbf{r}, \mathbf{r}_c^{1\mathfrak{b}})$ and $\mathcal{E}^+(\mathbf{r}, \mathbf{r}_c^{2\mathfrak{b}})$ can have splitting

$$\mathcal{E}^-(\mathbf{r}, \mathbf{r}_c^{1\mathfrak{b}}) = \mathcal{E}^-(\mathbf{r}_c^t, \mathbf{r}_c^{1\mathfrak{b}}) e^{i\mathbf{k}_\alpha \cdot (\boldsymbol{\rho}-\boldsymbol{\rho}_c^t)} e^{-k_\rho(z-z_c^t)},$$
$$\mathcal{E}^+(\mathbf{r}, \mathbf{r}_c^{2\mathfrak{b}}) = \mathcal{E}^+(\mathbf{r}_c^t, \mathbf{r}_c^{2\mathfrak{b}}) e^{i\mathbf{k}_\alpha \cdot (\boldsymbol{\rho}-\boldsymbol{\rho}_c^t)} e^{k_\rho(z-z_c^t)}.$$

Applying spherical harmonic expansion (2.37) again, we obtain

$$e^{i\mathbf{k}_\alpha \cdot (\boldsymbol{\rho}-\boldsymbol{\rho}_c^t)} e^{\pm k_\rho(z-z_c^t)} = \sum_{n=0}^{\infty} \sum_{m=-n}^{n} (\mp 1)^{n+m} C_n^m r_t^n Y_n^m(\theta_t, \varphi_t) k_\rho^n e^{-im\alpha}.$$

Substituting into (3.24), the ME is translated to LE (3.25) via

$$L_{nm}^{1\mathfrak{b}} = \sum_{n'=0}^{\infty} \sum_{m'=-n}^{n'} T_{nm,n'm'}^{1\mathfrak{b}} M_{n'm'}^{1\mathfrak{b}},$$

$$L_{nm}^{2\mathfrak{b}} = (-1)^{n+m} \sum_{n'=0}^{\infty} \sum_{m'=-n}^{n'} T_{nm,n'm'}^{2\mathfrak{b}} M_{n'm'}^{2\mathfrak{b}},$$

(3.29)

(a) $\tilde{u}_{11}^{11}(\boldsymbol{r}, \boldsymbol{r}'_{11})$

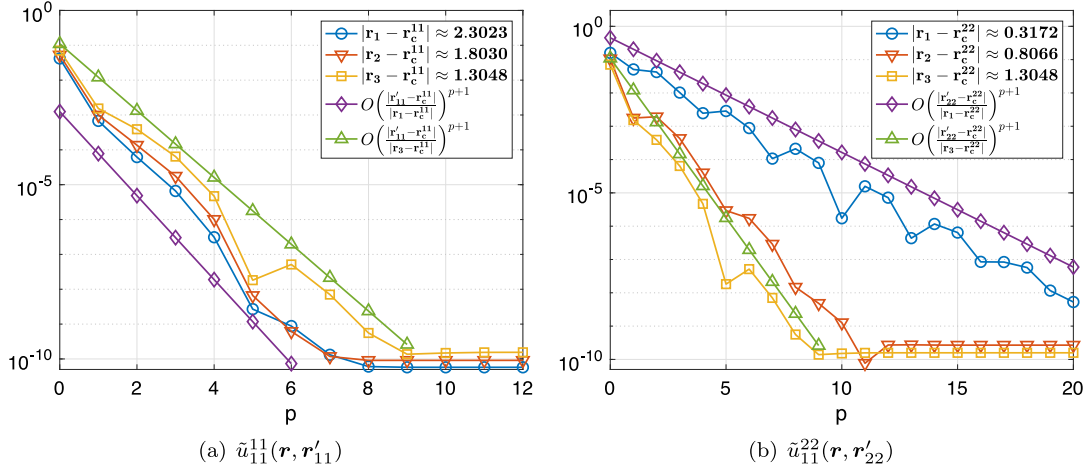(b) $\tilde{u}_{11}^{22}(\boldsymbol{r}, \boldsymbol{r}'_{22})$

Fig. 3.4. Spectral convergence of the MEs for reaction components.

Algorithm 1 FMM for general reaction component $\Phi_{\ell\ell'}^{\mathfrak{ab}}(\boldsymbol{r}_{\ell i})$, $i = 1, 2, \cdots, N_\ell$

Determine equivalent polarized coordinates for all source particles.

Generate an adaptive hierarchical tree structure according to polarization sources $\{Q_{\ell'j}, \boldsymbol{r}_{\ell'j}^{\mathfrak{ab}}\}_{j=1}^{N_{\ell'}}$ and targets $\{\boldsymbol{r}_{\ell i}\}_{i=1}^{N_\ell}$. Pre-compute $\{S^n I_{nm}^{\mathfrak{ab}}(\rho, z)\}_{n=0}^{2p}$ using recurrence formula (3.37) and DE-SE quadrature and formula (3.50) for initial values.

Upward pass:

for $l = H \to 0$ **do**

    for all boxes j on source tree level l **do**

        if j is a leaf node **then**

            form the free-space ME using Eq. (3.24).

        else

            form the free-space ME by merging children's expansions using the free-space center shift translation operator (2.19).

        end if

    end for

end for

Downward pass:

for $l = 1 \to H$ **do**

    for all boxes j on target tree level l **do**

        shift the LE of j's parent to j itself using the free-space shifting (2.20).

        collect interaction list contribution using the source box to target box translation operator in Eq. (3.29) while $T_{nm,n'm'}^{\mathfrak{ab}}$ are computed using (3.35) and pre-computed $\{S^n I_{nm}^{\mathfrak{ab}}(\rho, z)\}_{n=0}^{2p}$.

    end for

end for

Evaluate LEs:

for each leaf node (childless box) **do**

    evaluate the LE at each particle location.

end for

Local Direct Interactions:

for $i = 1 \to N$ **do**

    compute Eq. (3.16) of target particle i with sources in the neighboring boxes using the mixed DE-SE quadrature and formula (3.50) for $I_{00}^{\mathfrak{ab}}(\rho, z)$.

end for

---

and the M2L translation operators are given in integral forms as follows

$$T_{nm,n'm'}^{1\mathfrak{b}} = \frac{(-1)^{n'} D_{nm}^{n'm'}}{8\pi^2} \int_0^\infty \int_0^{2\pi} \mathcal{E}^-(\boldsymbol{r}_c^t, \boldsymbol{r}_c^{1\mathfrak{b}}) \sigma_{\ell\ell'}^{1\mathfrak{b}}(k_\rho) k_\rho^{n+n'} e^{\mathrm{i}(m'-m)\alpha} d\alpha \, dk_\rho,$$

$$T_{nm,n'm'}^{2\mathfrak{b}} = \frac{(-1)^{m'} D_{nm}^{n'm'}}{8\pi^2} \int_0^\infty \int_0^{2\pi} \mathcal{E}^+(\boldsymbol{r}_c^t, \boldsymbol{r}_c^{2\mathfrak{b}}) \sigma_{\ell\ell'}^{2\mathfrak{b}}(k_\rho) k_\rho^{n+n'} e^{\mathrm{i}(m'-m)\alpha} d\alpha \, dk_\rho,$$

(3.30)

where

$$D_{nm}^{n'm'} = c_{n'}^2 C_n^m C_{n'}^{m'}.$$

Again, the convergence of the Sommerfeld-type integrals in (3.30) requires the conditions in (3.28).

The framework of the traditional FMM together with ME (3.24), LE (3.25), M2L translation (3.29)–(3.30) and free space ME and LE center shifting (2.19) and (2.20) constitute the FMM for the computation of reaction components $\Phi_{\ell\ell'}^{\mathfrak{ab}}(\boldsymbol{r}_{\ell i})$, $\mathfrak{a}, \mathfrak{b} = 1, 2$. In the FMM for each reaction component, a large box is defined to include all equivalent polarization sources associated to the reaction component and corresponding target charges, and an adaptive tree structure will be built by a bisection procedure, see. Fig. 3.2. Note that the validity of the ME (3.24), LE (3.25) and M2L translation (3.29) used in the algorithm imposes restrictions (3.28) on the centers, accordingly. This can be ensured by setting the largest box for the specific reaction component to be equally divided by the interface between equivalent polarized sources and corresponding targets, see Fig. 3.2. Thus, the largest box for the FMM implementation will be different for different reaction components. With this setting, all source and target boxes of higher than zeroth level in the adaptive tree structure will have centers below or above the interfaces, accordingly. The fast multipole algorithm for the computation of a general reaction component $\Phi_{\ell\ell'}^{\mathfrak{ab}}(\boldsymbol{r}_{\ell i})$ is summarized in Algorithm 1. Total interactions given by (3.9) will be obtained by first calculating all components and then summing them up where the algorithm is presented in Algorithm 2.

3.4. Efficient computation of Sommerfeld-type integrals

It is clear that the FMM demands efficient computation of the double integrals involved in the MEs, LEs and M2L translations. In this section, we present an accurate and efficient way to

compute these double integrals. Firstly, the double integrals can be simplified by using the following identity

$$J_n(z) = \frac{1}{2\pi i^n} \int_0^{2\pi} e^{iz\cos\theta + in\theta} d\theta. \qquad (3.31)$$

Algorithm 2 3-D FMM for (3.9)

> **for** $\ell = 0 \to L$ **do**
>> use free space FMM to compute $\Phi_\ell^{free}(\boldsymbol{r}_{\ell i})$, $i = 1, 2, \cdots, N_\ell$.
>
> **end for**
> **for** $\ell = 0 \to L - 1$ **do**
>> **for** $\ell' = 0 \to L - 1$ **do**
>>> use **Algorithm 1** to compute $\Phi_{\ell\ell'}^{11}(\boldsymbol{r}_{\ell i})$, $i = 1, 2, \cdots, N_\ell$.
>>
>> **end for**
>> **for** $\ell' = 1 \to L$ **do**
>>> use **Algorithm 1** to compute $\Phi_{\ell\ell'}^{12}(\boldsymbol{r}_{\ell i})$, $i = 1, 2, \cdots, N_\ell$.
>>
>> **end for**
>
> **end for**
> **for** $\ell = 1 \to L$ **do**
>> **for** $\ell' = 0 \to L - 1$ **do**
>>> use **Algorithm 1** to compute $\Phi_{\ell\ell'}^{21}(\boldsymbol{r}_{\ell i})$, $i = 1, 2, \cdots, N_\ell$.
>>
>> **end for**
>> **for** $\ell' = 1 \to L$ **do**
>>> use **Algorithm 1** to compute $\Phi_{\ell\ell'}^{22}(\boldsymbol{r}_{\ell i})$, $i = 1, 2, \cdots, N_\ell$.
>>
>> **end for**
>
> **end for**

In particular, multipole expansion functions in (3.26) can be simplified as

$$\widetilde{\mathcal{F}}_{nm}^{1\mathfrak{b}}(\boldsymbol{r}, \boldsymbol{r}_c^{1\mathfrak{b}}) = \frac{(-1)^n c_n^2 C_n^m i^m e^{im\phi_s^{1\mathfrak{b}}}}{4\pi} \int_0^\infty J_m(k_\rho \rho_s^{1\mathfrak{b}}) e^{-k_\rho(z - z_c^{1\mathfrak{b}})} \sigma_{\ell\ell'}^{1\mathfrak{b}}(k_\rho) k_\rho^n dk_\rho,$$

$$\widetilde{\mathcal{F}}_{nm}^{2\mathfrak{b}}(\boldsymbol{r}, \boldsymbol{r}_c^{2\mathfrak{b}}) = \frac{(-1)^m c_n^2 C_n^m i^m e^{im\phi_s^{2\mathfrak{b}}}}{4\pi} \int_0^\infty J_m(k_\rho \rho_s^{2\mathfrak{b}}) e^{-k_\rho(z_c^{2\mathfrak{b}} - z)} \sigma_{\ell\ell'}^{2\mathfrak{b}}(k_\rho) k_\rho^n dk_\rho,$$

and the expression (3.27) for LE coefficients can be simplified as

$$L_{nm}^{1\mathfrak{b}} = \frac{(-1)^m C_n^m i^{-m} e^{-im\varphi_t^{1\mathfrak{b}}}}{4\pi} \int_0^\infty J_m(k_\rho \rho_t^{1\mathfrak{b}}) e^{-k_\rho(z_c^t - z'_{1\mathfrak{b}})} \sigma_{\ell\ell'}^{1\mathfrak{b}}(k_\rho) k_\rho^n dk_\rho,$$

$$L_{nm}^{2\mathfrak{b}} = \frac{(-1)^n C_n^m i^{-m} e^{-im\varphi_t^{2\mathfrak{b}}}}{4\pi} \int_0^\infty J_m(k_\rho \rho_t^{2\mathfrak{b}}) e^{-k_\rho(z'_{2\mathfrak{b}} - z_c^t)} \sigma_{\ell\ell'}^{2\mathfrak{b}}(k_\rho) k_\rho^n dk_\rho$$

for $\mathfrak{b} = 1, 2$, where $(\rho_s^{\mathfrak{ab}}, \varphi_s^{\mathfrak{ab}})$ and $(\rho_t^{\mathfrak{ab}}, \varphi_t^{\mathfrak{ab}})$ are polar coordinates of $\boldsymbol{r} - \boldsymbol{r}_c^{\mathfrak{ab}}$ and $\boldsymbol{r}_c^t - \boldsymbol{r}'_{\mathfrak{ab}}$ projected in the xy-plane, respectively. Moreover, the M2L translation (3.30) can be simplified as

$$T_{nm,n'm'}^{1\mathfrak{b}} = \frac{(-1)^{n'} \widetilde{D}_{nm}^{n'm'}(\varphi_{ts}^{1\mathfrak{b}})}{4\pi} \int_0^\infty k_\rho^{n+n'} J_{m'-m}(k_\rho \rho_{ts}^{1\mathfrak{b}}) e^{-k_\rho(z_c^t - z_c^{1\mathfrak{b}})} \sigma_{\ell\ell'}^{1\mathfrak{b}}(k_\rho) dk_\rho,$$

$$T_{nm,n'm'}^{2\mathfrak{b}} = \frac{(-1)^{m'} \widetilde{D}_{nm}^{n'm'}(\varphi_{ts}^{2\mathfrak{b}})}{4\pi} \int_0^\infty k_\rho^{n+n'} J_{m'-m}(k_\rho \rho_{ts}^{2\mathfrak{b}}) e^{-k_\rho(z_c^{2\mathfrak{b}} - z_c^t)} \sigma_{\ell\ell'}^{2\mathfrak{b}}(k_\rho) dk_\rho,$$

$$(3.32)$$

where $(\rho_{ts}^{\mathfrak{ab}}, \varphi_{ts}^{\mathfrak{ab}})$ is the polar coordinates of $\boldsymbol{r}_c^t - \boldsymbol{r}_c^{\mathfrak{ab}}$ projected in the xy plane,

$$\widetilde{D}_{nm}^{n'm'}(\varphi) = D_{nm}^{n'm'} i^{m'-m} e^{i(m'-m)\varphi}.$$

Define integral

$$I_{nm}^{\mathfrak{ab}}(\rho, z) := \int_0^\infty J_m(k_\rho \rho) \frac{k_\rho^n e^{-k_\rho z}}{\sqrt{(n+m)!(n-m)!}} \sigma_{\ell\ell'}^{\mathfrak{ab}}(k_\rho) dk_\rho, \qquad (3.33)$$

then

$$\widetilde{\mathcal{F}}_{nm}^{1\mathfrak{b}}(\boldsymbol{r}, \boldsymbol{r}_c^{1\mathfrak{b}}) = \frac{c_n e^{im\varphi_s^{1\mathfrak{b}}}}{4\pi} I_{nm}^{1\mathfrak{b}}(\rho_s^{1\mathfrak{b}}, z - z_c^{1\mathfrak{b}}),$$

$$L_{nm}^{1\mathfrak{b}} = \frac{(-1)^n}{4\pi c_n e^{im\varphi_t^{1\mathfrak{b}}}} I_{nm}^{1\mathfrak{b}}(\rho_t^{1\mathfrak{b}}, z_c^t - z'_{1\mathfrak{b}}),$$

$$(3.34)$$

$$\widetilde{\mathcal{F}}_{nm}^{2\mathfrak{b}}(\boldsymbol{r}, \boldsymbol{r}_c^{2\mathfrak{b}}) = \frac{(-1)^{n+m} c_n e^{im\varphi_s^{2\mathfrak{b}}}}{4\pi} I_{nm}^{2\mathfrak{b}}(\rho_s^{2\mathfrak{b}}, z_c^{2\mathfrak{b}} - z),$$

$$L_{nm}^{2\mathfrak{b}} = \frac{(-1)^m e^{-im\varphi_t^{2\mathfrak{b}}}}{4\pi c_n} I_{nm}^{2\mathfrak{b}}(\rho_t^{2\mathfrak{b}}, z'_{2\mathfrak{b}} - z_c^t),$$

$$T_{nm,n'm'}^{1\mathfrak{b}} = \frac{(-1)^{n+m} Q_{nm}^{n'm'} e^{i(m'-m)\varphi_{ts}^{1\mathfrak{b}}}}{4\pi} I_{n+n',m'-m}^{1\mathfrak{b}}(\rho_{ts}^{1\mathfrak{b}}, z_c^t - z_c^{1\mathfrak{b}}),$$

$$T_{nm,n'm'}^{2\mathfrak{b}} = \frac{(-1)^{n+m+n'+m'} Q_{nm}^{n'm'} e^{i(m'-m)\varphi_{ts}^{2\mathfrak{b}}}}{4\pi} I_{n+n',m'-m}^{2\mathfrak{b}}(\rho_{ts}^{2\mathfrak{b}}, z_c^{2\mathfrak{b}} - z_c^t),$$

$$(3.35)$$

where

$$Q_{nm}^{n'm'} := \sqrt{\frac{(2n'+1)(n+n'+m'-m)!(n+n'-m'+m)!}{(2n+1)(n+m)!(n-m)!(n'+m')!(n'-m')!}}.$$

Therefore, we actually need efficient algorithm for the computation of the Sommerfeld-type integrals $I_{nm}^{\mathfrak{ab}}(\rho, z)$ defined in (3.33). It is clearly that they have oscillatory integrands. These integrals are convergent when the target and source particles are not exactly on the interfaces of the layered medium. High order quadrature rules could be used for direct numerical computation at runtime. However, this becomes prohibitively expensive due to a large number of integrals needed in the FMM. In fact, $(p + 1)(2p + 1)$ integrals will be required for each source box to target box translation. Moreover, the involved integrand decays more slowly as n increases.

An important aspect in the implementation of FMM concerns scaling. Since $M_{nm}^{\mathfrak{ab}} \approx (|\boldsymbol{r} - \boldsymbol{r}_c^{\mathfrak{ab}}|)^n$, $L_{nm}^{\mathfrak{ab}} \approx (|\boldsymbol{r}^{\mathfrak{ab}} - \boldsymbol{r}_c^t|)^{-n}$, a naive use of the expansions (3.24) and (3.25) in the implementation of FMM is likely to encounter underflow and overflow issues. To avoid this, one must scale expansions, replacing M_{nm} with $M_{nm}^{\mathfrak{ab}}/S^n$ and L_{nm} with $L_{nm}^{\mathfrak{ab}} \cdot S^n$ where S is the scaling factor. To compensate for this scaling, we replace $\widetilde{\mathcal{F}}_{nm}^{\mathfrak{ab}}(\boldsymbol{r}, \boldsymbol{r}_c^{\mathfrak{ab}})$ with $\widetilde{\mathcal{F}}_{nm}^{\mathfrak{ab}}(\boldsymbol{r}, \boldsymbol{r}_c^{\mathfrak{ab}}) \cdot S^n$, $T_{nm,n'm'}^{\mathfrak{ab}}$ with $T_{nm,n'm'}^{\mathfrak{ab}} \cdot S^{n+n'}$. Usually, the scaling factor S is chosen to be the size of the box in which the computation occurs. Therefore, the following scaled Sommerfeld-type integrals

$$S^n I_{nm}^{\mathfrak{ab}}(\rho, z) = \int_0^\infty J_m(k_\rho \rho) \frac{(k_\rho S)^n e^{-k_\rho z} \sigma_{\ell\ell'}^{\mathfrak{ab}}(k_\rho)}{\sqrt{(n+m)!(n-m)!}} dk_\rho,$$

$$n \geq 0, \quad m = 0, 1, \ldots, n, \qquad (3.36)$$

are involved in the implementation of the FMM.

Recall the recurrence formula

$$J_{m+1}(z) = \frac{2m}{z} J_m(z) - J_{m-1}(z),$$

and define $a_n = \sqrt{n(n+1)}$. We have

$$S^n I_{nm+1}^{\mathfrak{ab}}(\rho, z) = \int_0^\infty J_{m+1}(k_\rho \rho) \frac{(k_\rho S)^n e^{-k_\rho z} \sigma_{\ell\ell'}^{\mathfrak{ab}}(k_\rho)}{\sqrt{(n+m+1)!(n-m-1)!}} dk_\rho$$

$$= \frac{2mS}{\rho} \int_0^\infty J_m(k_\rho \rho) \frac{(k_\rho S)^{n-1} e^{-k_\rho z} \sigma_{\ell\ell'}^{\mathfrak{ab}}(k_\rho)}{\sqrt{(n+m-1)!(n-m-1)!}}$$

$$\times \sqrt{\frac{(n+m-1)!}{(n+m+1)!}} dk_\rho$$

$$-\int_0^\infty J_{m-1}(k_\rho\rho)\frac{(k_\rho S)^n e^{-k_\rho z}\sigma_{\ell\ell'}^{\mathrm{ab}}(k_\rho)}{\sqrt{(n+m-1)!(n-m+1)!}}$$

$$\times\sqrt{\frac{(n+m-1)!(n-m+1)!}{(n+m+1)!(n-m-1)!}}\,dk_\rho,$$

which gives the forward recurrence formula

$$S^n I_{nm+1}^{\mathrm{ab}}(\rho,z)=\frac{2m}{a_{n+m}}\frac{S}{\rho}S^{n-1}I_{n-1m}^{\mathrm{ab}}(\rho,z)-\frac{a_{n-m}}{a_{n+m}}S^n I_{nm-1}^{\mathrm{ab}}(\rho,z),$$

$$(3.37)$$

for $m\geq 1, n\geq m+1$. The stability of this recurrence formula requires that

$$\frac{2m}{a_{n+m}}<\frac{\rho}{S}.\qquad(3.38)$$

In the computation of $\widetilde{\mathcal{F}}_{nm}^{\mathrm{ab}}(\boldsymbol{r},\boldsymbol{r}_c^{\mathrm{ab}})\cdot S^n$ and $L_{nm}^{\mathrm{ab}}\cdot S^n$, ρ_s^{ab} and ρ_t^{ab} could be arbitrary small. Therefore, the forward recurrence formula (3.37) may not be able to be applied to calculate them. Nevertheless, it is unnecessary to calculate $\widetilde{\mathcal{F}}_{nm}^{\mathrm{ab}}(\boldsymbol{r},\boldsymbol{r}_c^{\mathrm{ab}})\cdot S^n$ and $L_{nm}^{\mathrm{ab}}\cdot S^n$ directly in the FMM. The coefficients $L_{nm}^{\mathrm{ab}}\cdot S^n$ are calculated from ME coefficients via M2L translations and then the potentials are obtained via LEs (3.25). Therefore, we only need to consider the computation of the integrals involved in the M2L translation matrices $T_{nm,n'm'}^{\mathrm{ab}}$. For any polarization source box in the interaction list of a given target box, one can find that ρ_{ts}^{ab} is either 0 or larger than the box size S. If $\rho_{ts}^{\mathrm{ab}}=0$, we directly have

$$I_{nm}^{\mathrm{ab}}(\rho_{ts}^{\mathrm{ab}},z)=0,\quad\forall m>0,\ \ \forall z>0.\qquad(3.39)$$

In all other cases, we have $\rho_{ts}^{\mathrm{ab}}\geq S$ and the forward recurrence formula (3.37) can always be applied as we have

$$\frac{2m}{\sqrt{(n+m+1)(n+m)}}<\frac{1}{\sqrt{3}}<\frac{\rho_{ts}^{\mathrm{ab}}}{S},\quad n\geq m+1,\quad m\geq 1.$$

Given a truncation number p, we still need to use quadratures to calculate $4p+1$ initial values $\{I_{n0}^{\mathrm{ab}}(\rho,z)\}_{n=0}^{2p}$ and $\{I_{n1}^{\mathrm{ab}}(\rho,z)\}_{n=1}^{2p}$ for each M2L translation. Moreover, integrals $\{I_{00}^{\mathrm{ab}}(\rho,z)\}_{a,b=1}^2$ are also required in the computation of the direct interactions between particles in neighboring boxes. These calculations require an efficient and robust numerical method. Note that $\{I_{00}^{\mathrm{ab}}(\rho,z)\}_{a,b=1}^2$ are exactly the Sommerfeld integrals involved in the calculation of the layered Green's function. A multitude of papers have been published until now, devoted to their efficient calculation (see [25] and the references there in).

Basically, we will adopt the mixed DE-SE quadrature (cf. [25,26]) in this paper for efficient computations of the Sommerfeld-type integrals. Nevertheless, we still need to consider the case of large n which has not been covered in the literature. We have found that the formulation (3.36) is not adequate for two reasons: (i) the integrand may decay very slowly if z is small; (ii) the integrand may have increasing oscillating magnitude as n increases if $\rho>z$. As a matter of fact, the asymptotic formula (B.32) and

$$J_m(z)\sim\sqrt{\frac{2}{\pi z}}\cos\left(z-\frac{m\pi}{2}-\frac{\pi}{4}\right),\quad z\to\infty,$$

imply that the integrand in (3.36) has an asymptotic form

$$J_m(k_\rho\rho)\frac{(k_\rho S)^n e^{-k_\rho z}\sigma_{\ell\ell'}^{\mathrm{ab}}(k_\rho)}{\sqrt{(n+m)!(n-m)!}}\sim\sqrt{\frac{2}{\pi}}C_{\ell\ell'}^{\mathrm{ab}}\cos\left(k_\rho\rho-\frac{m\pi}{2}-\frac{\pi}{4}\right)$$

$$\times\frac{(k_\rho\rho)^{n-\frac{1}{2}}S^n e^{-k_\rho(z+\zeta_{\ell\ell'}^{\mathrm{ab}})}}{\sqrt{(n+m)!(n-m)!}},\qquad(3.40)$$

as $k_\rho\to\infty$. Given $\rho,z>0$, define

$$g_{nm}(k_\rho;\rho,z+\zeta_{\ell\ell'}^{\mathrm{ab}})=\frac{(k_\rho\rho)^{n-\frac{1}{2}}S^n e^{-k_\rho(z+\zeta_{\ell\ell'}^{\mathrm{ab}})}}{\sqrt{(n+m)!(n-m)!}},\qquad(3.41)$$

which has a maximum value

$$\max_{k_\rho\geq 0}g_{nm}(k_\rho;\rho,z+\zeta_{\ell\ell'}^{\mathrm{ab}})=\frac{S^n}{\sqrt{(n+m)!(n-m)!}}\left(\frac{2n-1}{2}\right)^{n-\frac{1}{2}}$$

$$\times\left(\frac{\rho}{z+\zeta_{\ell\ell'}^{\mathrm{ab}}}\right)^{n-\frac{1}{2}}e^{\frac{1}{2}-n},\qquad(3.42)$$

at $k_\rho=\frac{n}{z+\zeta_{\ell\ell'}^{\mathrm{ab}}}-\frac{1}{2(z+\zeta_{\ell\ell'}^{\mathrm{ab}})}$ for $n\geq 1$. Applying Stirling formula $n!\sim\sqrt{2\pi n}n^n/e^n$ yields

$$\max_{k_\rho\geq 0}g_{nm}(k_\rho;\rho,z+\zeta_{\ell\ell'}^{\mathrm{ab}})\sim\sqrt{\frac{(2n-1)e}{2}}$$

$$\times\frac{n!}{\sqrt{(n+m)!(n-m)!}}\left(\frac{\rho}{z+\zeta_{\ell\ell'}^{\mathrm{ab}}}\right)^{n-\frac{1}{2}}S^n,\quad\text{as}\quad n\to\infty.\quad(3.43)$$

Considering the case $m=0$ and setting $S=\sqrt{\rho^2+z^2}$, we have

$$\max_{k_\rho\geq 0}g_{n0}(k_\rho,\rho,z+\zeta_{\ell\ell'}^{\mathrm{ab}})\sim\sqrt{\frac{(2n-1)(z+\zeta_{\ell\ell'}^{\mathrm{ab}})e}{2\rho}}\left(\frac{\rho S}{z+\zeta_{\ell\ell'}^{\mathrm{ab}}}\right)^n$$

$$\geq\sqrt{\frac{(2n-1)(z+\zeta_{\ell\ell'}^{\mathrm{ab}})e}{2\rho}}\left(\frac{\rho^2}{z+\zeta_{\ell\ell'}^{\mathrm{ab}}}\right)^n,$$

$$\text{if}\ \ \rho>z+\zeta_{\ell\ell'}^{\mathrm{ab}}.$$

$$(3.44)$$

From the above estimate, we can see that the formulation (3.36) have very large cancellations in the integrand if $\rho/(z+\zeta_{\ell\ell'}^{\mathrm{ab}})$ and n are large, see Fig. 3.5(a) for an example. Therefore, simply applying a quadrature to formula (3.36) will not get correct results in all cases.

To overcome the problem discussed above, we will change the contour of the integral (3.36). For this purpose, let us first reformulate the integral (3.36) into

$$S^n I_{nm}^{\mathrm{ab}}(\rho,z)=\frac{1}{2}\int_0^\infty H_m^{(1)}(k_\rho\rho)\frac{(Sk_\rho)^n e^{-k_\rho z}}{\sqrt{(n+m)!(n-m)!}}\sigma_{\ell\ell'}^{\mathrm{ab}}(k_\rho)dk_\rho$$

$$-\frac{(-1)^m}{2}\int_{-\infty}^0 H_m^{(1)}(k_\rho\rho)\frac{(-Sk_\rho)^n e^{k_\rho z}}{\sqrt{(n+m)!(n-m)!}}\sigma_{\ell\ell'}^{\mathrm{ab}}(-k_\rho)dk_\rho,$$

$$(3.45)$$

by using identities

$$J_m(x)=\frac{H_m^{(1)}(x)+H_m^{(2)}(x)}{2},\quad H_m^{(2)}(-x)=(-1)^{m+1}H_m^{(1)}(x).\qquad(3.46)$$

According to the analysis in [27], the density function $\sigma_{\ell\ell'}^{\mathrm{ab}}(k_\rho)$ is analytic and bounded in the right half complex plane. Therefore, we can change the contour of the first integral from $[0,\infty)$ to $\Gamma_\xi^+:=\{k_\rho=\xi(1+\mathrm{i}),\xi>0\}$ and the contour of the second integral from $(-\infty,0]$ to $\Gamma_\xi^-:=\{k_\rho=\xi(1-\mathrm{i}),\xi<0\}$ to obtain

$$S^n I_{nm}^{\mathrm{ab}}(\rho,z)=\frac{1+\mathrm{i}}{2}\int_0^\infty H_m^{(1)}(\rho\xi(1+\mathrm{i}))$$

$$\times\frac{(S\xi)^n(1+\mathrm{i})^n e^{-z\xi(1+\mathrm{i})}}{\sqrt{(n+m)!(n-m)!}}\sigma_{\ell\ell'}^{\mathrm{ab}}((1+\mathrm{i})\xi)d\xi$$

$$-\frac{(-1)^m(1-\mathrm{i})}{2}\int_{-\infty}^0 H_m^{(1)}(\rho\xi(1-\mathrm{i}))$$

$$\times\frac{(-S\xi)^n(1-\mathrm{i})^n e^{z\xi(1-\mathrm{i})}}{\sqrt{(n+m)!(n-m)!}}\sigma_{\ell\ell'}^{\mathrm{ab}}((\mathrm{i}-1)\xi)d\xi.$$
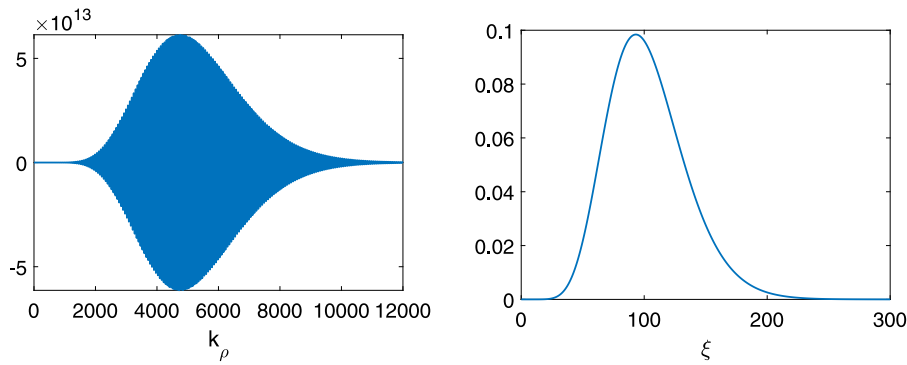
$$(3.47)$$

Fig. 3.5. A comparison of the integrand in (3.36) and the first integrand in (3.50) with $n = 10, m = 0, \rho = 0.1, z = 0.002$ and $\sigma_{11}^{11}(k_\rho)$ given in (B.35) ($d_0 = 0$, $d_1 = -1.2, \varepsilon_0 = 21.2, \varepsilon_1 = 47.5, \varepsilon_2 = 62.8$).

Recalling the asymptotic formulation (cf. [28, Eq. (10.7.8)])

$$H_m^{(1)}(z) \sim \frac{(1+i)}{\sqrt{\pi z}} e^{iz}, \quad z \to \infty, \quad -\pi + \delta \le \mathrm{ph} z \le 2\pi - \delta, \quad (3.48)$$

where δ is an arbitrary small positive number, we can obtain

$$H_m^{(1)}(\rho\xi(1+i)) \sim \frac{(1+i)}{\sqrt{\pi\rho\xi(1+i)}} e^{-\rho\xi} e^{i\rho\xi} \to 0, \quad \xi \to +\infty,$$

$$H_m^{(1)}(\rho\xi(1-i)) \sim \frac{(1+i)}{\sqrt{\pi\rho\xi(1-i)}} e^{\rho\xi} e^{i\rho\xi} \to 0, \quad \xi \to -\infty,$$

$$(3.49)$$

for all $\rho > 0$. Defining

$$G_{nm}^{ab}(\rho, z, \xi)$$
$$= \begin{cases} \dfrac{1+i}{2} H_m^{(1)}(\rho\xi(1+i)) \dfrac{(S\xi)^n(1+i)^n e^{-z\xi(1+i)}}{\sqrt{(n+m)!(n-m)!}} \\ \quad \times \sigma_{\ell\ell'}^{ab}((1+i)\xi), \quad \text{if } \xi \ge 0, \\ \dfrac{(-1)^m(i-1)}{2} H_m^{(1)}(\rho\xi(1-i)) \dfrac{(-S\xi)^n(1-i)^n e^{z\xi(1-i)}}{\sqrt{(n+m)!(n-m)!}} \\ \quad \times \sigma_{\ell\ell'}^{ab}((i-1)\xi), \quad \text{if } \xi < 0, \end{cases}$$

then, we have

$$S^n I_{nm}^{ab}(\rho, z) = \int_0^\infty G_{nm}^{ab}(\rho, z, \xi) d\xi + \int_0^\infty G_{nm}^{ab}(\rho, z, -\xi) d\xi. \quad (3.50)$$

By the asymptotic formulas (B.32) and (3.49), we have

$$G_{nm}^{ab}(\rho, z, \xi) \sim \frac{\xi^{n-\frac{1}{2}} S^n e^{-\xi(z+\rho+\zeta_{\ell\ell'}^{ab})}}{\sqrt{(n+m)!(n-m)!}}$$
$$= g_{nm}(\xi; 1, z + \rho + \zeta_{\ell\ell'}^{ab}), \quad \xi \to +\infty,$$
$$G_{nm}^{ab}(\rho, z, -\xi) \sim \frac{\xi^{n-\frac{1}{2}} S^n e^{-\xi(z+\rho+\zeta_{\ell\ell'}^{ab})}}{\sqrt{(n+m)!(n-m)!}}$$
$$= g_{nm}(\xi; 1, z + \rho + \zeta_{\ell\ell'}^{ab}), \quad \xi \to +\infty.$$
$$(3.51)$$

Recalling (3.43) to get

$$\max_{\xi \ge 0} g_{nm}(\xi; 1, \rho + z + \zeta_{\ell\ell'}^{ab}) \sim \sqrt{\frac{(2n-1)e}{2}}$$
$$\times \frac{n!}{\sqrt{(n+m)!(n-m)!}} \left(\frac{1}{\rho + z + \zeta_{\ell\ell'}^{ab}}\right)^{n-\frac{1}{2}} S^n. \quad (3.52)$$

As an example, we consider the case $m = 0$ and set $S = \sqrt{\rho^2 + z^2}$ again, i.e.,

$$\max_{\xi \ge 0} g_{n0}(\xi; 1, \rho + z + \zeta_{\ell\ell'}^{ab}) \sim \sqrt{\frac{(2n-1)e}{2(\rho + z + \zeta_{\ell\ell'}^{ab})}} \left(\frac{\sqrt{\rho^2 + z^2}}{\rho + z + \zeta_{\ell\ell'}^{ab}}\right)^n.$$
$$(3.53)$$

Apparently, the large cancellation in the case $\rho > z + \zeta_{\ell\ell'}^{ab}$ can be significantly suppressed by using the formulation (3.50). At the same time, the oscillating term $J_m(k_\rho\rho)$ is turned to be exponentially decaying functions $H_m^{(1)}(\rho\xi(1\pm i))$ and thus produce faster exponential decaying term. A comparison of the integrands in (3.36) and (3.50) are plotted in Fig. 3.5.

To end this section, we will give some numerical results to show the accuracy and efficiency of the algorithm using mixed DE-SE quadrature together with formulations (3.36) and (3.50) for the computation of the Sommerfeld type integrals. We test the integral with densities $\sigma_{\ell\ell'}^{ab}(k_\rho) \equiv 1$ as the asymptotic formula (B.32) implies that $\sigma_{\ell\ell'}^{ab}(k_\rho)$ tends to be either the constant $C_{\ell\ell'}^{ab}$ or 0 rapidly as $k_\rho \to \infty$. Letting $S = r := \sqrt{\rho^2 + z^2}$, then the identity (2.42) yields To end this section, we will give some numerical results to show the accuracy and efficiency of the algorithm using mixed DE-SE quadrature together with formulations (3.36) and (3.50) for the computation of the Sommerfeld type integrals. We test the integral with densities $\sigma_{\ell\ell'}^{ab}(k_\rho) \equiv 1$ as the asymptotic formula (B.32) implies that $\sigma_{\ell\ell'}^{ab}(k_\rho)$ tends to be either the constant $C_{\ell\ell'}^{ab}$ or 0 rapidly as $k_\rho \to \infty$. Letting $S = r := \sqrt{\rho^2 + z^2}$, then the identity (2.42) yields

$$r^n I_{nm}^{ab}(\rho, z) = \sqrt{\frac{4\pi}{2n+1}} \frac{1}{r} \widehat{P}_n^m\left(\frac{z}{r}\right). \quad (3.54)$$

We fix $z = 0.001$ and test $\rho = 0.0005, 0.01, 0.1$ by using two different quadratures: (i) the composite Gaussian quadrature applied to the integral (3.36); (ii) the mixed DE-SE quadrature applied to (3.50). For the composite Gaussian quadrature, the asymptotic formula (3.41) is used to determine the truncation points such that the magnitude of the integrand decays to smaller than $1.0e-15$. Then, a uniform mesh with mesh size equal to 2 and 30 Gauss points in each interval is used to achieve machine accuracy in regular cases. Due to the small value of z, a very large truncation is needed if the formulation (3.36) is used. The numerical results are compared in Table 3.1, while the reference values are calculated by (3.54). We can see that the integral domain truncation is larger than 47834 for the composite Gauss quadrature approach when $\rho = 0.0005, n = 5$ and $m = 0, 1$. The truncations in all other tested cases are even larger. Thus, a large number of quadrature points have to be used to achieve a

Table 3.1
A comparison of two quadrature rules for the computation of Sommerfeld integrals with $z = 0.001$.

ρ	n	m	Composite Gauss		Mixed DE-SE	
			Number of points	Error	Number of points	Error
0.0005	5	0	717523	$-3.307\mathrm{e}{-12}$	52	$7.105\mathrm{e}{-14}$
		1	716016	$2.576\mathrm{e}{-11}$	52	$1.421\mathrm{e}{-14}$
	10	0	892278	$6.954\mathrm{e}{-12}$	72	$-2.842\mathrm{e}{-14}$
		1	891431	$1.882\mathrm{e}{-11}$	72	$-9.059\mathrm{e}{-14}$
0.01	5	0	872989	$-1.427\mathrm{e}{-10}$	56	$4.441\mathrm{e}{-16}$
		1	871511	$-2.716\mathrm{e}{-11}$	64	$3.108\mathrm{e}{-15}$
	10	0	1246898	$1.147\mathrm{e}{-5}$	56	$-1.443\mathrm{e}{-15}$
		1	1246090	$-6.755\mathrm{e}{-6}$	56	$6.883\mathrm{e}{-15}$
0.1	5	0	1039851	$-8.793\mathrm{e}{-7}$	72	$7.632\mathrm{e}{-17}$
		1	1038393	$-9.250\mathrm{e}{-7}$	72	$-4.996\mathrm{e}{-16}$
	10	0	1610764	-10615.95	48	$1.943\mathrm{e}{-16}$
		1	1609974	1334.402	48	$2.775\mathrm{e}{-17}$

good accuracy when the composite Gauss quadrature is applied to (3.36). In contrast, the mixed DE-SE quadrature can obtain machine accuracy using no more than 100 points. Moreover, as the ratio ρ/z increases, applying composite Gauss quadrature to (3.36) cannot produce reasonable results due to the large cancellation in (3.36). Instead, the mixed DE-SE quadrature applied to (3.50) can still provide results with almost machine accuracy using no more than 100 quadrature points.

Remark 3.1. In the FMM for reaction components, the most time consuming part is still the computation of the M2L matrices. Nevertheless, the equations in (3.35) show that we can pre-compute $\{S^n I_{nm}^{ab}(\rho, z)\}_{n=0}^{2p}, m = 0, 1, \ldots, n$ for all possible (ρ, z) determined by the target box and all source boxes in its interaction list. As target and equivalent polarization source boxes are always separated by a material interface, we only have no more than 29 different (ρ, z) cases for all M2L in a fixed level of the tree structure. Denoted the depth of the tree structure used in the FMM by H, then the total number of pre-computed matrices is equal to $29H$.

4. Numerical results

In this section, we present numerical results to demonstrate the performance of the proposed FMM. The algorithm is implemented based on an open-source adaptive FMM package DASHMM (cf. [29]) on a workstation with two Xeon E5-2699 v4 2.2 GHz processors (each has 22 cores) and 500GB RAM using the GCC compiler version 6.3. The main improvement in the numerical results compared with that presented in [19] for the Helmholtz equation is that no off-line computation is needed and numerical tests with media of many layers and charges very close to interfaces are presented.

Charges in a 3 layer medium. We first test problems in a three layers medium with interfaces placed at $z_0 = 0$, $z_1 = -1.2$. Charges are set to be uniformly distributed in irregular domains which are obtained by shifting the domain determined by $r = 0.599 - a + \frac{a}{8}(35 \cos^4 \theta - 30 \cos^2 \theta + 3)$ with $a = 0.1, 0.15, 0.05$ to new centers $(0, 0, 0.6)$, $(0, 0, -0.6)$ and $(0, 0, -1.8)$, respectively (see Fig. 4.1(a) for the cross section of the domains). Particle locations are generated randomly with a uniform distribution in a larger cube within corresponding irregular domains. We can see that the minimum distance between charges and the interfaces is 0.001 in all three layers, i.e., the numerical examples have charges very close to the interfaces. In the layered medium, the material parameters are set to be $\varepsilon_0 = 21.2$, $\varepsilon_1 = 47.5$, $\varepsilon_2 = 62.8$. Let $\widetilde{\Phi}_\ell(\mathbf{r}_{\ell i})$ be the approximated values of $\Phi_\ell(\mathbf{r}_{\ell i})$ calculated by FMM.

Table 4.1
Comparison of CPU time (sec) using multiple cores ($p = 5$).

cores	N	time for all $\{\Phi_\ell^{free}\}_{\ell=0}^2$	time for all $\{\Phi_{\ell\ell'}^{ab}\}$
1	4164016	426.66	67.76
	6229016	436.30	57.75
	8883960	455.32	75.97
	12202880	527.56	132.06
6	4164016	80.78	21.86
	6229016	82.96	20.76
	8883960	86.54	25.74
	12202880	100.08	42.94
36	4164016	24.97	20.58
	6229016	25.71	18.81
	8883960	26.02	23.45
	12202880	28.51	36.72

Define ℓ^2 and maximum errors as

$$
Err_2^\ell := \sqrt{\frac{\sum_{i=1}^{N_\ell} |\Phi_\ell(\mathbf{r}_{\ell i}) - \widetilde{\Phi}_\ell(\mathbf{r}_{\ell i})|^2}{\sum_{i=1}^{N_\ell} |\Phi_\ell(\mathbf{r}_{\ell i})|^2}},
$$
$$
Err_{max}^\ell := \max_{1 \le i \le N_\ell} \frac{|\Phi_\ell(\mathbf{r}_{\ell i}) - \widetilde{\Phi}_\ell(\mathbf{r}_{\ell i})|}{|\Phi_\ell(\mathbf{r}_{\ell i})|}.
\tag{4.1}
$$

For accuracy test, we put $N = 1168 + 856 + 1504$ charges in the irregular domains in three layers, see Fig. 4.1(a). Convergence rates against p are depicted in Fig. 4.1(b). Clearly, the proposed FMM has an exponential convergence with respect to the truncation order p. The CPU time for the computation of all three free space components $\{\Phi_\ell^{free}(\mathbf{r}_{\ell i})\}_{\ell=0}^2$ and sixteen reaction components $\Phi_{\ell\ell'}^{ab}(\mathbf{r}_{\ell i})$ with fixed truncation number $p = 5$ are compared in Fig. 4.1(c) for up to 12 millions charges. It shows that all of them have an $O(N)$ complexity while the CPU time for the computation of reaction components is much shorter than that for free space components due to the fact that most of the equivalent polarization sources are well-separated from the targets. The CPU times with multiple cores are given in Table 4.1 and they show that the speedup of the parallel computing for reaction components is lower than that for the free space components as the pre-computation for the matrices $\{S^n I_{nm}^{ab}(\rho, z)\}_{n=0}^{2p}$ has not been implemented in parallel. Here, we only use parallel implementation within the FMM for each component. Note that the computation of each component is independent of all other components. Therefore, it is straightforward to implement a version of the code which computes all components in parallel.

Charges in solar cell media with up to 32 layers. Next, to test a more practical problem and also to check the scaling of the algorithm with respect to the number of layers (L), we consider
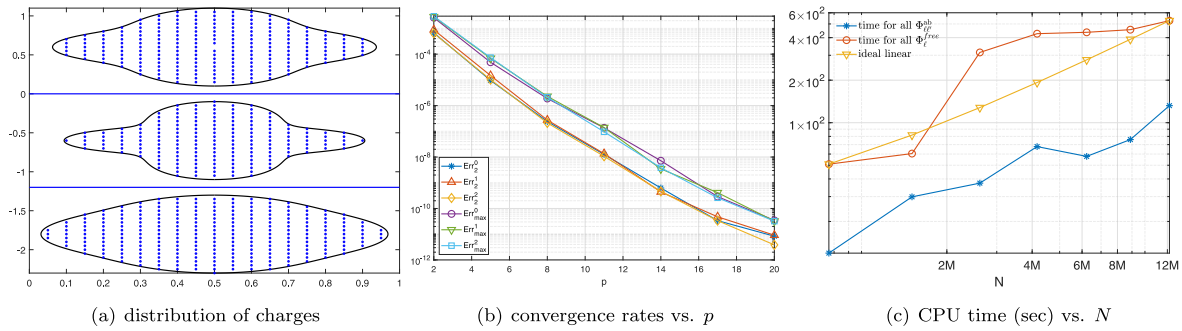
(a) distribution of charges   (b) convergence rates vs. p (c) CPU time (sec) vs. N

Fig. 4.1. Performance of FMM for problem in a three layers medium.

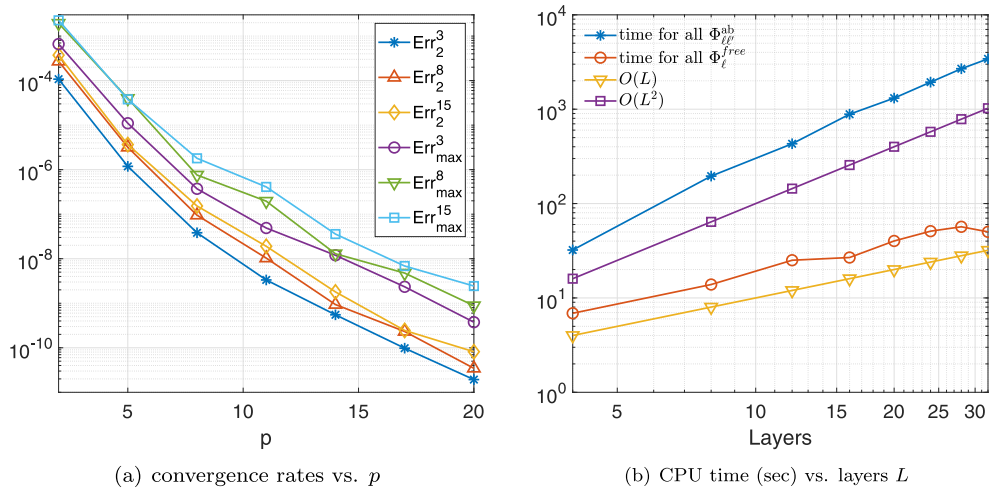(a) convergence rates vs. p (b) CPU time (sec) vs. layers L

Fig. 4.2. Performance of FMM for problems in media with many layers.

a typical layout of a multi-layered solar cell (cf. [30]) where the main components are Gallium Arsenide (GaAs), Indium Arsenide (InAs) and Silicon (Si), which have relative dielectric constants 12.9, 15.15 and 2.4, respectively. We will test different cases with up to 32 layers and 32 million charges. In each case, the width of the layers is fixed to be 1.2 and three materials: GaAs, InAs and Si are randomly selected in the layered structure. Moreover, the source charges are randomly picked in cubic box of size 1 in each layer. For accuracy test, we consider a medium with 16 layers and put 1000 randomly selected source charges in each box. Therefore, the total number of charges is 16 000. The errors of the potentials in the 3th, 8th and 15th layers are depicted in Fig. 4.2(a). We can see that highly accurate results can be obtained with p less than 20. To show the dependence of the CPU time on the number of layers L, we test examples of different L and put 1 million randomly selected source charges in each layer. Multiple cores (40 cores) are used and the CPU time is depicted in Fig. 4.2(b). The results show that the FMM can handle large number of sources in many layers efficiently. According to the derivation in Appendix B, the number of free space and reaction field components are L and $4(L^2 - 2L + 1)$, respectively, when a L-layers medium is considered. Therefore, the CPU time for free space and reaction field components is $O(L)$ and $O(L^2)$ as we can see in Fig. 4.2(b). Moreover, it is worthy to point out that the computation of all reaction components are independent from each other, hence can be done in parallel.

5. Conclusion

In this paper, we have presented a fast multipole method for the efficient calculation of the interactions between charged particles embedded in 3-D layered media. The layered media Green's function of the Laplace equation is decomposed into a free space and four types of reaction components. The associated equivalent polarization sources are introduced to re-express the reaction components. New MEs and LEs of $O(p^2)$ terms for the far field of the reaction components and M2L translation operators are derived, accordingly. As a result, the traditional FMM framework can be applied to both the free space and reaction components once the polarization sources are used together with the original sources. For systems of large number of charges, the computational cost from the reaction components is only a fraction of that of the FMM for the free space components. Therefore, computing the interactions of many sources in layered media basically costs the same as that for the interactions in the free space and the proposed FMM scales as $O(N)$ in terms of the number of charges N in a layered medium and $O(L^2)$ in terms of the number of layers L.

For the future work, we will carry out error estimate of the FMM for the Laplace equation in 3-D layered media, which requires careful analysis for the convergence of the new MEs and M2L operators for the reaction components. The application of the FMM in capacitance extraction of interconnects in VLSI will also be considered in a future work.

Declaration of competing interest

The authors declare that they have no known competing financial interests or personal relationships that could have appeared to influence the work reported in this paper.

Acknowledgments

Appendix A. Addition theorems

The following presents the addition theorems (cf. [12,31]), which have been used for the derivation of the ME, LE and corresponding shifting and translation operators of the free space Green's function. Here we adopt the definition

$$
Y_n^m(\theta, \varphi) = (-1)^m \sqrt{\frac{2n+1}{4\pi} \frac{(n-m)!}{(n+m)!}} P_n^m(\cos\theta) e^{im\varphi} := \widehat{P}_n^m(\cos\theta) e^{im\varphi},
$$
(A.1)

for the spherical harmonics where $P_n^m(x)$ (resp. $\widehat{P}_n^m(x)$) is the associated (resp. normalized) Legendre function of degree n and order m. Recall that

$$
P_n^m(x) = (-1)^m (1-x^2)^{\frac{m}{2}} \frac{d^m}{dx^m} P_n(x)
$$
(A.2)

for integer order $0 \le m \le n$ and

$$
P_n^{-m} = (-1)^m \frac{(n-m)!}{(n+m)!} P_n^m(x), \quad \text{so} \quad \widehat{P}_n^{-m}(x) = (-1)^m \widehat{P}_n^m(x)
$$
(A.3)

for $0 < m \le n$, where $P_n(x)$ is the Legendre polynomial of degree n. The so-defined spherical harmonics constitute a complete orthogonal basis of $L(\mathbb{S}^2)$ (where $\mathbb{S}^2$ is the unit spherical surface) and

$$
\langle Y_n^m, Y_{n'}^{m'} \rangle = \delta_{nn'} \delta_{mm'}, \quad Y_n^{-m}(\theta, \varphi) = (-1)^m \overline{Y_n^m(\theta, \varphi)}.
$$

It is worthy to point out that the spherical harmonics with different scaling constant defined as

$$
\widetilde{Y}_n^m(\theta, \varphi) = \sqrt{\frac{(n-|m|)!}{(n+|m|)!}} P_n^{|m|}(\cos\theta) e^{im\varphi} = i^{m+|m|} \sqrt{\frac{4\pi}{2n+1}} Y_n^m(\theta, \varphi),
$$
(A.4)

have been frequently adopted in published FMM papers (e.g., [12, 21]). By using the spherical harmonics defined in (A.1) and constants

$$
c_n = \sqrt{\frac{2n+1}{4\pi}}, \quad A_n^m = \frac{(-1)^n c_n}{\sqrt{(n-m)!(n+m)!}}, \quad |m| \le n,
$$
(A.5)

the addition theorems in [12,31] can be represented as:

Theorem A.1 (*Addition Theorem for Legendre Polynomials*)**.** *Let P and Q be points with spherical coordinates (r, θ, φ) and (ρ, α, β), respectively, and let γ be the angle subtended between them. Then*

$$
P_n(\cos\gamma) = \frac{4\pi}{2n+1} \sum_{m=-n}^{n} \overline{Y_n^m(\alpha, \beta)} Y_n^m(\theta, \varphi).
$$
(A.6)

Theorem A.2. *Let $Q = (\rho, \alpha, \beta)$ be the center of expansion of an arbitrary spherical harmonic of negative degree. Let the point $P = (r, \theta, \varphi)$, with $r > \rho$, and $P - Q = (r', \theta', \varphi')$. Then*

$$
\frac{Y_{n'}^{m'}(\theta', \varphi')}{r'^{n'+1}} = \sum_{n=0}^{\infty} \sum_{m=-n}^{n} \frac{(-1)^m A_n^m A_{n'}^{m'} \rho^n Y_n^{-m}(\alpha, \beta)}{c_n^2 A_{n+n'}^{m+m'}} \frac{Y_{n+n'}^{m+m'}(\theta, \varphi)}{r^{n+n'+1}}.
$$

Theorem A.3. *Let $Q = (\rho, \alpha, \beta)$ be the center of expansion of an arbitrary spherical harmonic of negative degree. Let the point $P = (r, \theta, \varphi)$, with $r < \rho$, and $P - Q = (r', \theta', \varphi')$. Then*

$$
\frac{Y_{n'}^{m'}(\theta', \varphi')}{r'^{n'+1}} = \sum_{n=0}^{\infty} \sum_{m=-n}^{n} \frac{(-1)^{n'+m} A_n^m A_{n'}^{m'} \cdot Y_{n+n'}^{m'-m}(\alpha, \beta)}{c_n^2 A_{n+n'}^{m'-m} \rho^{n+n'+1}} r^n Y_n^m(\theta, \varphi).
$$

Theorem A.4. *Let $Q = (\rho, \alpha, \beta)$ be the center of expansion of an arbitrary spherical harmonic of negative degree. Let the point $P = (r, \theta, \varphi)$ and $P - Q = (r', \theta', \varphi')$. Then*

$$
r'^{n'} Y_{n'}^{m'}(\theta', \varphi') = \sum_{n=0}^{n'} \sum_{m=-n}^{n} \frac{(-1)^n c_{n'}^2 A_n^m A_{n'-n}^{m'-m} \cdot \rho^n Y_n^m(\alpha, \beta)}{c_n^2 c_{n'-n}^2 A_{n'}^{m'} r^{n-n'}} Y_{n'-n}^{m'-m}(\theta, \varphi),
$$

where $A_n^m = 0$, $Y_n^m(\theta, \varphi) \equiv 0$ for $|m| > n$ is used.

Appendix B. A stable recursive algorithm for computing reaction densities

Denote the solution of the problem (3.1)–(3.2) in the ℓth layer by $u_{\ell\ell'}(\boldsymbol{r}, \boldsymbol{r}')$ and its partial Fourier transform along $x-$ and $y-$directions by

$$
\widehat{u}_{\ell\ell'}(k_x, k_y, z) = \mathscr{F}[u_{\ell\ell'}(\boldsymbol{r}, \boldsymbol{r}')](k_x, k_y, z)
$$
$$
:= \int_{-\infty}^{\infty} \int_{-\infty}^{\infty} u_{\ell\ell'}(\boldsymbol{r}, \boldsymbol{r}') e^{-i(k_x x + k_y y)} dx dy.
$$

Then, $\widehat{u}_{\ell\ell'}(k_x, k_y, z)$ satisfies second order ordinary differential equation

$$
\frac{d^2 \widehat{u}_{\ell\ell'}(k_x, k_y, z)}{dz^2} - k_\rho^2 \widehat{u}_{\ell\ell'}(k_x, k_y, z) = -e^{-i(k_x x' + k_y y')} \delta(z, z'), \quad z \ne d_\ell.
$$
(B.1)

Here, we consider the following general interface conditions

$$
a_{\ell-1} \widehat{u}_{\ell-1, \ell'}(k_x, k_y, z) = a_\ell \widehat{u}_{\ell\ell'}(k_x, k_y, z),
$$
$$
b_{\ell-1} \frac{d\widehat{u}_{\ell-1, \ell'}(k_x, k_y, z)}{dz} = b_\ell \frac{d\widehat{u}_{\ell\ell'}(k_x, k_y, z)}{dz},
$$
(B.2)

in the frequency domain for $\ell = 1, 2, \ldots, L$, where $\{a_\ell, b_\ell\}$ are given constants. Apparently, the classic transmission condition (3.2) will lead to a special case of (B.2) with $a_\ell = 1$, $b_\ell = \varepsilon_\ell$. In the top and bottom-most layers, we also have decaying condition

$$
\widehat{u}_{0\ell'}(k_x, k_y, z) \to 0, \quad \widehat{u}_{L\ell'}(k_x, k_y, z) \to 0, \quad \text{as } z \to \pm\infty.
$$
(B.3)

This interface problem has a general solution

$$
\begin{cases}
\widehat{u}_{0\ell'}(k_x, k_y, z) = \sigma_{0\ell'}^1 e^{-k_\rho(z-d_0)}, \\
\widehat{u}_{\ell'\ell'}(k_x, k_y, z) = \sigma_{\ell'\ell'}^1 e^{-k_\rho(z-d_{\ell'})} \\
\quad + \sigma_{\ell'\ell'}^2 e^{-k_\rho(d_{\ell'-1}-z)} + \delta_{\ell\ell'} \widehat{G}(k_x, k_y, z, z'), \\
\widehat{u}_{L\ell'}(k_x, k_y, z) = \sigma_{L\ell'}^2 e^{-k_\rho(d_{L-1}-z)},
\end{cases}
$$
(B.4)

where $\delta_{\ell\ell'}$ is the Kronecker symbol, and

$$
\widehat{G}(k_x, k_y, z, z') = \vartheta e^{-k_\rho |z-z'|}, \quad \vartheta = \frac{e^{-i(k_x x' + k_y y')}}{2k_\rho},
$$
(B.5)

is the Fourier transform of the free space Green's function. We will use the decomposition

$$
\widehat{G}(k_x, k_y, z, z') = \widehat{G}^1(k_x, k_y, z, z') + \widehat{G}^2(k_x, k_y, z, z'),
$$
(B.6)

where the two components are defined as

$$\widehat{G}^1(k_x, k_y, z, z') := H(z' - z)\vartheta\, e^{-k_\rho(z'-z)},$$
$$\widehat{G}^2(k_x, k_y, z, z') := H(z - z')\vartheta\, e^{-k_\rho(z-z')}, \tag{B.7}$$

and $H(x)$ is the Heaviside function.

We first consider the ℓth layer without source ($\ell \neq \ell'$), where the right hand side of (B.1) becomes zero, the solution is given by

$$\widehat{u}_{\ell\ell'}(k_x, k_y, z) = \sigma^1_{\ell\ell'}(k_x, k_y)e^{-k_\rho(z-d_\ell)} + \sigma^2_{\ell\ell'}(k_x, k_y)e^{-k_\rho(d_{\ell-1}-z)}. \tag{B.8}$$

Applying the interface condition (B.2) at $z = d_{\ell-1}$ gives

$$a_{\ell-1}\sigma^1_{\ell-1,\ell'} + a_{\ell-1}e^{-k_\rho D_{\ell-1}}\sigma^2_{\ell-1,\ell'} = a_\ell e^{-k_\rho D_\ell}\sigma^1_{\ell\ell'} + a_\ell\sigma^2_{\ell\ell'},$$
$$b_{\ell-1}\sigma^1_{\ell-1,\ell'} - b_{\ell-1}e^{-k_\rho D_{\ell-1}}\sigma^2_{\ell-1,\ell'} = b_\ell e^{-k_\rho D_\ell}\sigma^1_{\ell\ell'} - b_\ell\sigma^2_{\ell\ell'}, \tag{B.9}$$

or in matrix form

$$\widehat{\mathbb{S}}^{(\ell-1)}\begin{pmatrix}\sigma^1_{\ell-1,\ell'} \\ \sigma^2_{\ell-1,\ell'}\end{pmatrix} = \widetilde{\mathbb{S}}^{(\ell)}\begin{pmatrix}\sigma^1_{\ell\ell'} \\ \sigma^2_{\ell\ell'}\end{pmatrix}, \tag{B.10}$$

where

$$\widehat{\mathbb{S}}^{(\ell)} := \begin{pmatrix}a_\ell & a_\ell e_\ell \\ b_\ell & -b_\ell e_\ell\end{pmatrix}, \quad \widetilde{\mathbb{S}}^{(\ell)} := \begin{pmatrix}a_\ell e_\ell & a_\ell \\ b_\ell e_\ell & -b_\ell\end{pmatrix}, \quad \ell = 2, 3, \ldots, L-1, \tag{B.11}$$

and

$$e_\ell := e^{-k_\rho D_\ell}, \quad d_{-1} := d_0,$$
$$d_{L+1} := d_L, \quad D_\ell = d_{\ell-1} - d_\ell, \quad \ell = 0, 1, \ldots, L. \tag{B.12}$$

Solving the above equations for $\{\sigma^1_{\ell-1,\ell'}, \sigma^2_{\ell-1,\ell'}\}$, we obtain

$$\begin{pmatrix}\sigma^1_{\ell-1,\ell'} \\ \sigma^2_{\ell-1,\ell'}\end{pmatrix} = \mathbb{T}^{\ell-1,\ell}\begin{pmatrix}\sigma^1_{\ell\ell'} \\ \sigma^2_{\ell\ell'}\end{pmatrix} \tag{B.13}$$

for $\ell = 2, 3, \ldots, L-1$, where

$$\mathbb{T}^{\ell-1,\ell} = \begin{pmatrix}a_{\ell-1} & a_{\ell-1}e_{\ell-1} \\ b_{\ell-1} & -b_{\ell-1}e_{\ell-1}\end{pmatrix}^{-1}\begin{pmatrix}a_\ell e_\ell & a_\ell \\ b_\ell e_\ell & -b_\ell\end{pmatrix}$$
$$= \frac{1}{2e_{\ell-1}}\begin{pmatrix}e_{\ell-1} & 0 \\ 0 & 1\end{pmatrix}\widehat{\mathbb{T}}^{\ell-1,\ell}\begin{pmatrix}e_\ell & 0 \\ 0 & 1\end{pmatrix}, \tag{B.14}$$

and

$$\widehat{\mathbb{T}}^{\ell-1,\ell} := \begin{pmatrix}\dfrac{a_\ell}{a_{\ell-1}} + \dfrac{b_\ell}{b_{\ell-1}} & \dfrac{a_\ell}{a_{\ell-1}} - \dfrac{b_\ell}{b_{\ell-1}} \\[2mm] \dfrac{a_\ell}{a_{\ell-1}} - \dfrac{b_\ell}{b_{\ell-1}} & \dfrac{a_\ell}{a_{\ell-1}} + \dfrac{b_\ell}{b_{\ell-1}}\end{pmatrix}. \tag{B.15}$$

For the top and bottom most layers, we have $\sigma^\downarrow_{0\ell'} = 0$ and $\sigma^\uparrow_{L\ell'} = 0$, we can also verify that

$$\begin{pmatrix}\sigma^1_{0\ell'} \\ 0\end{pmatrix} = \mathbb{T}^{01}\begin{pmatrix}\sigma^1_{1\ell'} \\ \sigma^2_{1\ell'}\end{pmatrix}, \quad \begin{pmatrix}\sigma^1_{L-1,\ell'} \\ \sigma^2_{L-1,\ell'}\end{pmatrix} = \mathbb{T}^{L-1,L}\begin{pmatrix}0 \\ \sigma^2_{L\ell'}\end{pmatrix}. \tag{B.16}$$

Next, we consider the solution in the layer with source $\boldsymbol{r}'$ inside, i.e., the solution in the ℓ'th layer. The general solution is given by

$$\widehat{u}_{\ell'\ell'}(k_x, k_y, z) = \sigma^1_{\ell'\ell'}e^{ik_{\ell'}z(z-d_{\ell'})} + \sigma^2_{\ell'\ell'}e^{ik_{\ell'}z(d_{\ell'-1}-z)} + \widehat{G}(k_x, k_y, z, z'). \tag{B.17}$$

At the interfaces $z = d_{\ell'-1}$ and $z = d_{\ell'}$, the interface conditions (B.2) lead to equations

$$a_{\ell'-1}\left(\sigma^1_{\ell'-1,\ell'} + e_{\ell'-1}\sigma^2_{\ell'-1,\ell'}\right) = a_{\ell'}\left(e_{\ell'}\sigma^1_{\ell'\ell'} + \sigma^2_{\ell'\ell'} + \widehat{G}^2(k_x, k_y, d_{\ell'-1}, z')\right),$$
$$b_{\ell'-1}\left(\sigma^1_{\ell'-1,\ell'} - e_{\ell'-1}\sigma^2_{\ell'-1,\ell'}\right) = b_{\ell'}\left(e_{\ell'}\sigma^1_{\ell'\ell'} - \sigma^2_{\ell'\ell'}\right) - \frac{b_{\ell'}}{k_\rho}\partial_z\widehat{G}^2(k_x, k_y, d_{\ell'-1}, z'), \tag{B.18}$$

and

$$a_{\ell'}\left(\sigma^1_{\ell'\ell'} + e_{\ell'}\sigma^2_{\ell'\ell'}\right) = a_{\ell'+1}\left(e_{\ell'+1}\sigma^1_{\ell'+1\ell'} + \sigma^2_{\ell'+1,\ell'}\right) - a_{\ell'}\widehat{G}^1(k_x, k_y, d_{\ell'}, z'),$$
$$b_{\ell'}\left(\sigma^1_{\ell'\ell'} - e_{\ell'}\sigma^2_{\ell'\ell'}\right) = b_{\ell'+1}\left(e_{\ell'+1}\sigma^1_{\ell'+1\ell'} - \sigma^2_{\ell'+1,\ell'}\right) + \frac{b_{\ell'}}{k_\rho}\partial_z\widehat{G}^1(k_x, k_y, d_{\ell'}, z'). \tag{B.19}$$

Note that

$$\partial_z\widehat{G}^2(k_x, k_y, d_{\ell'-1}, z') = -k_\rho\widehat{G}^2(k_x, k_y, d_{\ell'-1}, z'),$$
$$\partial_z\widehat{G}^1(k_x, k_y, d_{\ell'}, z') = k_\rho\widehat{G}^1(k_x, k_y, d_{\ell'}, z').$$

Then, Eqs. (B.18)–(B.19) can be reformulated as

$$\begin{pmatrix}\sigma^1_{\ell'-1,\ell'} \\ \sigma^2_{\ell'-1,\ell'}\end{pmatrix} = \mathbb{T}^{\ell'-1,\ell'}\begin{pmatrix}\sigma^1_{\ell'\ell'} \\ \sigma^2_{\ell'\ell'}\end{pmatrix} + \breve{\mathbb{S}}^{(\ell'-1)}\begin{pmatrix}a_{\ell'} \\ b_{\ell'}\end{pmatrix}\widehat{G}^2(k_x, k_y, d_{\ell'-1}, z') \tag{B.20}$$

and

$$\begin{pmatrix}\sigma^1_{\ell'\ell'} \\ \sigma^2_{\ell'\ell'}\end{pmatrix} = \mathbb{T}^{\ell'\ell'+1}\begin{pmatrix}\sigma^1_{\ell'+1,\ell'} \\ \sigma^2_{\ell'+1,\ell'}\end{pmatrix} + \breve{\mathbb{S}}^{(\ell')}\begin{pmatrix}-a_{\ell'} \\ b_{\ell'}\end{pmatrix}\widehat{G}^1(k_x, k_y, d_{\ell'}, z'), \tag{B.21}$$

where

$$\breve{\mathbb{S}}^{(\ell)} = \left(\widehat{\mathbb{S}}^{(\ell)}\right)^{-1} = \frac{1}{2}\begin{pmatrix}1 & 0 \\ 0 & e_\ell^{-1}\end{pmatrix}\begin{pmatrix}\dfrac{1}{a_\ell} & \dfrac{1}{b_\ell} \\[2mm] \dfrac{1}{a_\ell} & -\dfrac{1}{b_\ell}\end{pmatrix} := \begin{pmatrix}\breve{S}^{(\ell)}_{11} & \breve{S}^{(\ell)}_{12} \\ \breve{S}^{(\ell)}_{21} & \breve{S}^{(\ell)}_{22}\end{pmatrix}. \tag{B.22}$$

Define

$$\widetilde{\mathbb{T}}^{\ell-1,\ell} = 2e_{\ell-1}\mathbb{T}^{\ell-1,\ell}, \quad C^{(\ell)} = \prod_{j=0}^{\ell-1}\frac{1}{2e_j},$$
$$\mathbb{A}^{(\ell)} = \widetilde{\mathbb{T}}^{01}\widetilde{\mathbb{T}}^{12}\cdots\widetilde{\mathbb{T}}^{\ell-1,\ell} := \begin{pmatrix}\alpha^{(\ell)}_{11} & \alpha^{(\ell)}_{12} \\ \alpha^{(\ell)}_{21} & \alpha^{(\ell)}_{22}\end{pmatrix}, \tag{B.23}$$

for $\ell = 1, 2, \ldots, L$. Then, recursions in (B.13), (B.20) and (B.21) result in the system

$$\begin{pmatrix}\sigma^1_{0\ell'} \\ 0\end{pmatrix} = C^{(L)}\mathbb{A}^{(L)}\begin{pmatrix}0 \\ \sigma^2_{L\ell'}\end{pmatrix} + C^{(\ell'-1)}\mathbb{A}^{(\ell'-1)}\breve{\mathbb{S}}^{(\ell'-1)}\begin{pmatrix}a_{\ell'} \\ b_{\ell'}\end{pmatrix}\widehat{G}^2(k_x, k_y, d_{\ell'-1}, z')$$
$$+ C^{(\ell')}\mathbb{A}^{(\ell')}\breve{\mathbb{S}}^{(\ell')}\begin{pmatrix}-a_{\ell'} \\ b_{\ell'}\end{pmatrix}\widehat{G}^1(k_x, k_y, d_{\ell'}, z'). \tag{B.24}$$

It is not numerically stable to directly solve (B.24) for $\sigma^1_{0\ell'}$ and $\sigma^2_{L\ell'}$ then apply recursions (B.13), (B.20) and (B.21) to obtain all other reaction densities due to the exponential functions involved in the formulations. According to the expression (B.14), the recursions (B.13), (B.20) and (B.21) are stable for the computation of

the components $\sigma_{\ell\ell'}^1(k_\rho)$. As for the computation of the components $\sigma_{\ell\ell'}^2(k_\rho)$, we need to form linear systems similar as (B.24) using recursions (B.13), (B.20) and (B.21) and then solve it.

We first solve the second equation in (B.24) to get

$$\sigma_{L\ell'}^2 = \sigma_{L\ell'}^{21}\widehat{G}^1(k_x, k_y, d_{\ell'}, z') + \sigma_{L\ell'}^{22}\widehat{G}^2(k_{\ell'z}, d_{\ell'-1}, z'),$$

where

$$\sigma_{L\ell'}^{21} = -\frac{C^{(\ell'+1)}}{C^{(L)}\alpha_{22}^{(L)}} \begin{pmatrix} \alpha_{21}^{(\ell')} & \alpha_{22}^{(\ell')} \end{pmatrix} 2e_{\ell'}\breve{\mathbb{S}}^{(\ell')} \begin{pmatrix} -a_{\ell'} \\ b_{\ell'} \end{pmatrix}, \quad 0 \le \ell' < L,$$

$$\sigma_{L\ell'}^{22} = -\frac{C^{(\ell')}}{C^{(L)}\alpha_{22}^{(L)}} \begin{pmatrix} \alpha_{21}^{(\ell'-1)} & \alpha_{22}^{(\ell'-1)} \end{pmatrix} 2e_{\ell'-1}\breve{\mathbb{S}}^{(\ell'-1)} \begin{pmatrix} a_{\ell'} \\ b_{\ell'} \end{pmatrix}, \quad 0 < \ell' \le L.$$

(B.25)

According to the recursion (B.13), (B.20) and (B.21), all other reaction densities also have decompositions

$$\sigma_{\ell\ell'}^1 = \sigma_{\ell\ell'}^{11}\widehat{G}^1(k_x, k_y, d_{\ell'}, z') + \sigma_{\ell\ell'}^{12}\widehat{G}^2(k_x, k_y, d_{\ell'-1}, z'),$$
$$\sigma_{\ell\ell'}^2 = \sigma_{\ell\ell'}^{21}\widehat{G}^1(k_x, k_y, d_{\ell'}, z') + \sigma_{\ell\ell'}^{22}\widehat{G}^2(k_x, k_y, d_{\ell'-1}, z').$$

(B.26)

For each $0 \le \ell < L$, we first calculate $\{\sigma_{\ell\ell'}^{11}, \sigma_{\ell\ell'}^{12}\}$ by using one of the recursions (B.13), (B.20) and (B.21), then formulate a linear system for $\{\sigma_{0\ell'}^1, \sigma_{\ell\ell'}^2\}$ as the linear system (B.24). Next, we solve the second equation in the linear system to obtain reaction densities $\{\sigma_{\ell\ell'}^{21}, \sigma_{\ell\ell'}^{22}\}$. In summary, the formulations are given as follows:

$$\sigma_{\ell\ell'}^{11} = \begin{cases} T_{11}^{\ell'\ell'+1}\sigma_{\ell'+1,\ell'}^{11} + T_{12}^{\ell'\ell'+1}\sigma_{\ell'+1,\ell'}^{21} \\ \quad -\breve{S}_{11}^{(\ell')}a_{\ell'} + \breve{S}_{12}^{(\ell')}b_{\ell'}, & \ell = \ell', \\ T_{11}^{\ell\ell+1}\sigma_{\ell+1,\ell'}^{11} + T_{12}^{\ell\ell+1}\sigma_{\ell+1,\ell'}^{21}, & \text{else,} \end{cases}$$

(B.27)

$$\sigma_{\ell\ell'}^{12} = \begin{cases} T_{11}^{\ell'-1,\ell'}\sigma_{\ell'\ell'}^{12} + T_{12}^{\ell'-1,\ell'}\sigma_{\ell'\ell'}^{22} + \breve{S}_{11}^{(\ell'-1)}a_{\ell'} \\ \quad +\breve{S}_{12}^{(\ell'-1)}b_{\ell'}, & \ell = \ell' - 1, \\ T_{11}^{\ell\ell+1}\sigma_{\ell+1,\ell'}^{12} + T_{12}^{\ell\ell+1}\sigma_{\ell+1,\ell'}^{22}, & \text{else,} \end{cases}$$

(B.28)

$$\sigma_{\ell\ell'}^{21} = \begin{cases} -\dfrac{1}{\alpha_{22}^{(\ell)}} \begin{pmatrix} 0 & 1 \end{pmatrix} \left[\dfrac{C^{(\ell'+1)}}{C^{(\ell)}}\mathbb{A}^{(\ell)}2e_{\ell'}\breve{\mathbb{S}}^{(\ell')} \right. \\ \quad \left. \times \begin{pmatrix} -a_{\ell'} \\ b_{\ell'} \end{pmatrix} + \mathbb{A}^{(\ell)} \begin{pmatrix} \sigma_{\ell\ell'}^{11} \\ 0 \end{pmatrix} \right], & \ell > \ell', \\ -\dfrac{\alpha_{21}^{(\ell)}}{\alpha_{22}^{(\ell)}}\sigma_{\ell\ell'}^{11}, & \text{else,} \end{cases}$$

(B.29)

$$\sigma_{\ell\ell'}^{22} = \begin{cases} -\dfrac{1}{\alpha_{22}^{(\ell)}} \begin{pmatrix} 0 & 1 \end{pmatrix} \left[\dfrac{C^{(\ell')}}{C^{(\ell)}}\mathbb{A}^{(\ell-1)}2e_{\ell'-1} \right. \\ \quad \left. \breve{\mathbb{S}}^{(\ell'-1)} \begin{pmatrix} a_{\ell'} \\ b_{\ell'} \end{pmatrix} + \mathbb{A}^{(\ell)} \begin{pmatrix} \sigma_{\ell\ell'}^{12} \\ 0 \end{pmatrix} \right], & \ell \ge \ell', \\ -\dfrac{\alpha_{21}^{(\ell)}}{\alpha_{22}^{(\ell)}}\sigma_{\ell\ell'}^{12}, & \text{else.} \end{cases}$$

(B.30)

Substituting (B.26) and (B.7) into (B.4) and taking inverse Fourier transform, we obtain expressions (3.3)–(3.7).

From the definition (B.14) and (B.23), we have

$$T_{11}^{\ell\ell+1} = \frac{a_{\ell+1}b_\ell + a_\ell b_{\ell+1}}{2a_\ell b_\ell}e_{\ell+1}, \quad T_{12}^{\ell\ell+1} = \frac{a_{\ell+1}b_\ell - a_\ell b_{\ell+1}}{2a_\ell b_\ell},$$

$$2e_\ell\breve{\mathbb{S}}^{(\ell)} = \begin{pmatrix} a_\ell^{-1}e_\ell & b_\ell^{-1}e_\ell \\ a_\ell^{-1} & -b_\ell^{-1} \end{pmatrix},$$

$$\frac{C^{(\ell_1)}}{C^{(\ell_2)}} = \begin{cases} 1 & \ell_1 = \ell_2, \\ 2^{\ell_2-\ell_1}e^{-k_\rho(d_{\ell_1-1}-d_{\ell_2-1})} & 0 \le \ell_1 < \ell_2, \end{cases}$$

and an asymptotic behavior

$$\mathbb{A}^{(\ell)} \sim \begin{pmatrix} \tilde{\alpha}_{11}^{(\ell)}e_0e_1\cdots e_\ell & \tilde{\alpha}_{12}^{(\ell)}e_0 \\ \tilde{\alpha}_{21}^{(\ell)}e_\ell & \tilde{\alpha}_{22}^{(\ell)} \end{pmatrix}, \quad k_\rho \to \infty,$$

(B.31)

where $\{\tilde{\alpha}_{11}^{(\ell)}, \tilde{\alpha}_{12}^{(\ell)}, \tilde{\alpha}_{21}^{(\ell)}, \tilde{\alpha}_{22}^{(\ell)}\}$ are constants independent of k_ρ. By using these formulations in (B.25)–(B.30), we can show that all reaction densities $\{\sigma_{\ell\ell'}^{ab}(k_\rho)\}_{a,b=1}^2$ have an asymptotic behavior

$$\sigma_{\ell\ell'}^{ab}(k_\rho) \sim C_{\ell\ell'}^{ab}e^{-k_\rho\zeta_{\ell\ell'}^{ab}}, \quad k_\rho \to \infty,$$

(B.32)

where $C_{\ell\ell'}^{ab}$ and $\zeta_{\ell\ell'}^{ab}$ are constants independent of k_ρ. For example, we have

$$\sigma_{L\ell'}^{21}(k_\rho) \sim 2^{L-\ell'-1}\frac{\tilde{\alpha}_{22}^{(\ell')}}{\alpha_{22}^{(L)}}e^{-k_\rho(d_{\ell'}-d_{L-1})}, \quad k_\rho \to \infty,$$

$$\sigma_{L\ell'}^{22}(k_\rho) \sim 2^{L-\ell'}\frac{\alpha_{22}^{(\ell')}}{\alpha_{22}^{(L)}}\left(\frac{a_{\ell'}}{a_{\ell'-1}} + \frac{b_{\ell'}}{b_{\ell'-1}}\right)e^{-k_\rho(d_{\ell'-1}-d_{L-1})}, \quad k_\rho \to \infty.$$

(B.33)

If the number of layers is not large, we are able to write down explicit expressions of the reaction densities. Here, we give expressions for the case of a three layers media with $a_\ell = 1$, $b_\ell = \varepsilon_\ell$ as an example.

- Source in the top layer:

$$\sigma_{00}^{11}(k_\rho) = \frac{(\varepsilon_0 - \varepsilon_1)(\varepsilon_1 + \varepsilon_2) + (\varepsilon_0 + \varepsilon_1)(\varepsilon_1 - \varepsilon_2)e^{2d_1k_\rho}}{2\kappa(k_\rho)},$$

$$\sigma_{10}^{21}(k_\rho) = \frac{\varepsilon_0(\varepsilon_1 + \varepsilon_2)}{\kappa(k_\rho)}, \quad \sigma_{10}^{11}(k_\rho) = \frac{\varepsilon_0(\varepsilon_1 - \varepsilon_2)e^{d_1k_\rho}}{\kappa(k_\rho)},$$

$$\sigma_{20}^{21}(k_\rho) = \frac{2\varepsilon_0\varepsilon_1e^{d_1k_\rho}}{\kappa(k_\rho)}.$$

(B.34)

- Source in the middle layer:

$$\sigma_{01}^{12}(k_\rho) = \frac{\varepsilon_1(\varepsilon_1 + \varepsilon_2)}{\kappa(k_\rho)}, \quad \sigma_{01}^{11}(k_\rho) = \frac{\varepsilon_1(\varepsilon_1 - \varepsilon_2)e^{d_1k_\rho}}{\kappa(k_\rho)},$$

$$\sigma_{11}^{11}(k_\rho) = \frac{(\varepsilon_1 - \varepsilon_2)(\varepsilon_1 + \varepsilon_0)}{2\kappa(k_\rho)}, \quad \sigma_{11}^{21}(k_\rho) = \frac{(\varepsilon_1 - \varepsilon_2)(\varepsilon_1 - \varepsilon_0)e^{d_1k_\rho}}{2\kappa(k_\rho)},$$

$$\sigma_{11}^{12}(k_\rho) = \frac{(\varepsilon_1 - \varepsilon_2)(\varepsilon_1 - \varepsilon_0)e^{d_1k_\rho}}{2\kappa(k_\rho)}, \quad \sigma_{11}^{22}(k_\rho) = \frac{(\varepsilon_1 + \varepsilon_2)(\varepsilon_1 - \varepsilon_0)}{2\kappa(k_\rho)},$$

$$\sigma_{21}^{22}(k_\rho) = \frac{\varepsilon_1(\varepsilon_1 - \varepsilon_0)e^{d_1k_\rho}}{\kappa(k_\rho)}, \quad \sigma_{21}^{21}(k_\rho) = \frac{\varepsilon_1(\varepsilon_0 + \varepsilon_1)}{\kappa(k_\rho)}.$$

(B.35)

- Source in the bottom layer:

$$\sigma_{02}^{12}(k_\rho) = \frac{2\varepsilon_1\varepsilon_2e^{d_1k_\rho}}{\kappa(k_\rho)},$$

$$\sigma_{12}^{22}(k_\rho) = \frac{\varepsilon_2(\varepsilon_1 - \varepsilon_0)e^{d_1k_\rho}}{\kappa(k_\rho)}, \quad \sigma_{12}^{12}(k_\rho) = \frac{\varepsilon_2(\varepsilon_0 + \varepsilon_1)}{\kappa(k_\rho)},$$

$$\sigma_{22}^{22}(k_\rho) = \frac{(\varepsilon_1 - \varepsilon_0)(\varepsilon_1 + \varepsilon_2) + (\varepsilon_0 + \varepsilon_1)(\varepsilon_2 - \varepsilon_1)e^{2d_1k_\rho}}{2\kappa(k_\rho)},$$

(B.36)

where

$$\kappa(k_\rho) = \frac{1}{2}\big[(\varepsilon_0 + \varepsilon_1)(\varepsilon_1 + \varepsilon_2) + (\varepsilon_0 - \varepsilon_1)(\varepsilon_2 - \varepsilon_1)e^{2d_1k_\rho}\big].$$

Apparently, these expressions also verify our conclusion (B.32) on the asymptotic behavior of the reaction densities.

References

[1] W. Yu, X. Wang, Advanced Field-Solver Techniques for RC Extraction of Integrated Circuits, Springer, 2014.

[2] A. Seidl, H. Klose, M. Svoboda, J. Oberndorfer, W. Rosner, IEEE Trans. Comput. Aided Des. 7 (5) (1988) 549–556.

[3] A.E. Ruehli, P.A. Brennan, IEEE Trans. Microw. Theory Tech. 21 (2) (1973) 76–82.

[4] K.S. Oh, D. Kuznetsov, J.E. Schuttaine, IEEE Trans. Microw. Theory Tech. 42 (8) (1994) 1443–1453.

[5] J.S. Zhao, W.M. Dai, S. Kadur, D.E. Long, Proceedings of the 35th Annual Design Automation Conference, 1998, pp. 224–229.

[6] S.L. Campbell, I.C. Ipsen, C.T. Kelley, C.D. Meyer, BIT Numer. Math. 36 (4) (1996) 664–675.

[7] M. Xu, R.R. Alfano, Opt. Lett. 30 (22) (2005) 3051–3053.

[8] I. Babuska, G. Caloz, J.E. Osborn, SIAM J. Numer. Anal. 31 (4) (1994) 945–981.

[9] L. Borcea, Inverse Problems 18 (6) (2002) R99–R136.

[10] K. Nabors, J.K. White, IEEE Trans. Comput. Aided Des. 10 (11) (1991) 1447–1459.

[11] L. Greengard, V. Rokhlin, J. Comput. phys. 73 (2) (1987) 325–348.

[12] L. Grengard, V. Rokhlin, The Rapid Evaluation of Potential Fields in Three Dimensions, Research Report YALEU/DCS/RR-515, Dept. of Comp. Sci. Yale University, Springer, New Haven, CT, 1987.

[13] Y.L. Chow, J.J. Yang, D.G. Fang, G.E. Howard, IEEE Trans. Microw. Theory Tech. 39 (3) (1991) 588–592.

[14] M.I. Aksun, IEEE Trans. Microw. Theory Tech. 44 (5) (1996) 651–658.

[15] A. Alparslan, M.I. Aksun, K.A. Michalski, IEEE Trans. Microw. Theory Tech. 58 (3) (2010) 602–613.

[16] V. Jandhyala, E. Michielssen, R. Mittra, Int. J. Microw. Millimet. Wave Comput. Aided Eng. 5 (2) (1995) 68–78.

[17] L. Gurel, M.I. Aksun, IEEE Microw. Guid. W. 6 (8) (1996) 277.

[18] N. Geng, A. Sullivan, L. Carin, IEEE Trans. Antennas Propag. 49 (5) (2001) 740–748.

[19] B. Wang, W.Z. Zhang, W. Cai, SIAM J. Sci. Comput. 41 (6) (2019) A3954–A3981.

[20] W. Zhang, B. Wang, W. Cai, Exponential convergence for multipole expansion and translation to local expansions for sources in layered media: 2-D acoustic wave. arXiv:SIAM Numer. Anal. (2020) in press.

[21] L. Greengard, V. Rokhlin, Acta Numer. 6 (1997) 229–269.

[22] W. Cai, Computational Methods for Electromagnetic Phenomena: Electrostatics in Solvation, Scattering, and Electron Transport, Cambridge University Press, New York, NY, 2013.

[23] G. Watson, A Treatise of the Theory of Bessel Functions, second ed., Cambridge University Press, Cambridge, UK, 1966.

[24] P.A. Martin, Multiple Scattering: Interaction of Time-Harmonic Waves with N Obstacles, No. 107, Cambridge University Press, 2006.

[25] K.A. Michalski, J.R. Mosig, J. Electromagn. Waves Appl. 30 (3) (2016) 281–317.

[26] H. Takahasi, M. Mori, Double Exponential Formulas for Numerical Integration, Vol. 9, (3) Publ. RIMS, Kyoto Univ., 1974, pp. 721–741.

[27] B. Wang, W.Z. Zhang, W. Cai, Exponential convergence for multipole and local expansions and their translations for sources in layered media: three-dimensional Laplace equation, 2020, arXiv:2008.00571.

[28] F.W.J. Olver, NIST Handbook of Mathematical Functions, Cambridge University Press, 2010.

[29] J. DeBuhr, B. Zhang, A. Tsueda, V. Tilstra-Smith, T. Sterling, Commun. Comput. Phys. 20 (4) (2016) 1106–1126.

[30] K.A. Sablon, J.W. Little, V. Mitin, A. Sergeev, N. Vagidov, K. Reinhardt, Nano Lett. 11 (6) (2011) 2311–2317.

[31] M.A. Epton, B. Dembart, SIAM J. Sci. Comput. 16 (4) (1995) 865–897.